# CLIMATE CHANGE & FLOODING in SNOHOMISH COUNTY:

## New Dynamically Downscaled Hydrologic Model Projections

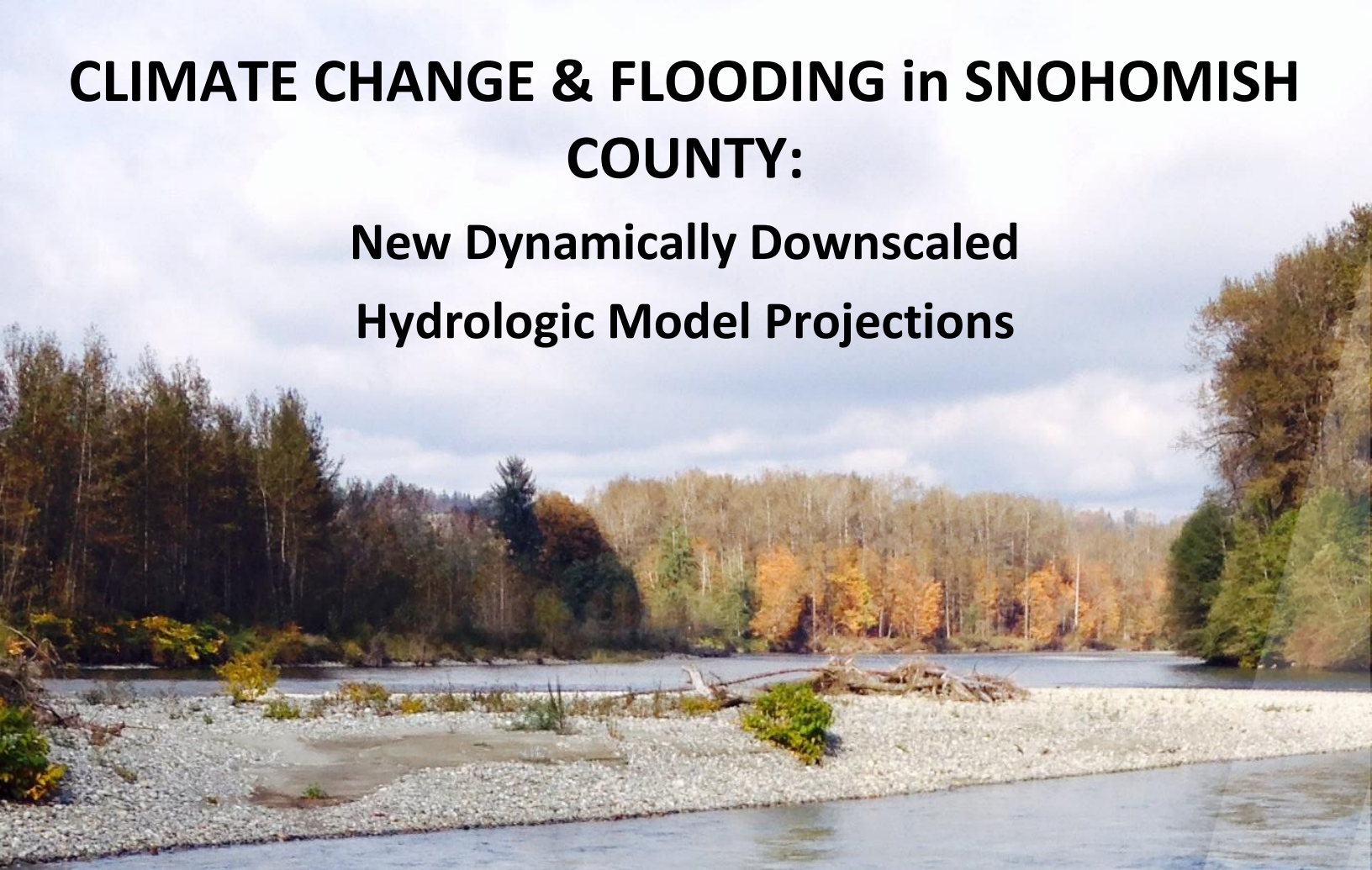


GUILLAUME MAUGER | UW CIG

JAMES ROBINSON | WWU

ROBERT MITCHELL | WWU

JASON WON | UW CIG

NICOLETA CRISTEA | UW CEE


JULY 2021

Photo by Flickr user Grant Matthews:

*South Fork Stillaguamish. Photo Credit: James Robinson*

**COVER PAGE PHOTO CREDIT:** Snohomish R. by Tom Sparks, used CC BY-NC-ND 2.0

**ACKNOWLEDGEMENTS:**

This work was supported by Snohomish County through a grant from the Washington State Floodplains by Design Program, the Stillaguamish Tribe, and by the U.S. Geological Survey Northwest Climate Adaptation Science Center award G17AC000218 to James Robinson. Regional climate model simulations were provided by Ruby Leung at Pacific Northwest National Laboratory and Cliff Mass in the UW Department of Atmospheric Sciences.

**CITATION:**

Mauger, G.S., J. Robinson, R.J. Mitchell, J. Won, and N. Cristea (2021). New Flood Projections for Snohomish County: Fine-scale Modeling and Dynamically-Downscaling. Report prepared for Snohomish County. Climate Impacts Group, University of Washington.

# TABLE OF CONTENTS

## Executive Summary

Climate change is projected to exacerbate river flooding for two primary reasons: (1) declining snowpack (e.g., Mote et al. 2018), and (2) more intense heavy rain events (e.g., Warner et al. 2015). Past studies have accounted for changes in snowpack but did not accurately capture changes in rainfall intensity. The purpose of this project was to develop new projections of future streamflow, with a particular emphasis on flooding, for the Snohomish and Stillaguamish Rivers.

We calibrated the Distributed Hydrology Soil Vegetation Model (DHSVM; Wigmosta et al. 1994) to the Snohomish and Stillaguamish River basins using dynamically downscaled historical meteorological data. Hydrology projections were simulated with the calibrated DHSVM models using a new ensemble of 12 regional climate model projections (Lorente-Plazas et al. 2018), which previous studies have shown to more accurately represent changes in heavy rain intensities (e.g., Salathé et al. 2014). We evaluated changes in flood peaks for several durations (1-hour, 1-day, 3-day, 7-day) and return intervals (2-, 5-, 10-, 20-, 25-, 50-, and 100-year events).

The model average projections show increases in flooding in both basins for all of the above durations and return intervals, without exception. Specifically: our results indicate that peak flows will increase substantially – ranging from about +10 to +40%, on average, by the 2080s – depending on the river location, duration, and return interval in question. Our results show a tendency for larger changes for longer duration flood events, and the range among models tends to also be higher for longer duration events. The results do not show a clear relationship with return interval (e.g., 2-year vs 100-year events).

It is difficult to detect trends in rare events. For this reason we expect that the projections for the 2-, 5-, and 10-year events will be most reliable. Similarly, our methods are not likely to provide reliable estimates of changes for the 1.01-year and 500-year events. We nonetheless provide projections for these events, for reference, but recommend against using them in planning or design decisions.

All model results and select flow statistics can be obtained from the project website: https://cig.uw.edu/projects/climate-change-flooding-in-snohomish-county-new-dynamically-downscaled-hydrologic-model-projections/

## Introduction and Background

In the Puget Sound region, climate change is expected to impact flooding via three primary mechanisms: sea level rise, more intense heavy rains, and reduced snowpack. Snow influences flood risk by increasing the amount of precipitation falling as rain during winter storms (see, e.g.: Mauger et al. 2015). Other factors are also expected to affect flood risk, such as wildfires and increased sediment deposition in rivers. Acting together, the changes are likely to be consequential. The purpose of this project was to develop new projections of future streamflow, with a particular emphasis on flooding, for the Snohomish and Stillaguamish Rivers. The Snohomish results of this study were the basis for the climate change hydraulic modeling in WSE (2020) and Cardno (2021).

This project leverages existing modeling by the University of Washington Climate Impacts Group (UW CIG) and Western Washington University (WWU) on both the Snohomish and Stillaguamish Rivers, respectively. Specifically, King County funded significant work developing improved estimates of future weather conditions -- using new regional climate model projections -- as well as calibrated fine-scale hydrologic models of the Green and Snohomish River basins. Similarly, the Stillaguamish Tribe of Indians contracted with WWU to develop projections of future streamflow and stream temperature in the North and South Forks of the Stillaguamish River. This existing work is lacking in three key respects: (1) the approaches for the two river basins are not sufficiently compatible to allow an apples-to-apples comparison of risks, (2) additional work is needed to refine and improve the meteorological inputs to the hydrologic simulations, and (3) new regional climate model simulations have now become available; these can be used to improve the characterization of future conditions. These improvements, as well as the resulting projections, are described in the text that follows.

## Methods

### Climate Data

This section describes the "downscaled" global climate model (GCM) projections used in the current study, and how they were validated and bias-corrected for use in the hydrologic modeling. As noted above, recent research has emphasized the need to use regional climate model projections (or "dynamical downscaling") in order to better quantify changes in extreme precipitation (e.g., Salathé et al. 2014). In this work we made use of existing regional climate model simulations, all performed using the Weather Research and Forecasting model (WRF; Skamarock et al. 2005). Key features of the WRF simulations used in this project are summarized in Table 1; these are described in greater depth in the sections that follow.

**Table 1.** Dynamically-downscaled Weather Research and Forecasting (WRF) model simulations used in the current study.

| Name | Type | Source | Bdry. Cond. | # of Sims | Time Step | Spatial Res. | Years |
|---|---|---|---|---|---|---|---|
| **WRF-OBS** | Historical | PNNL | NARR | 1 | 1 hr | 6 km | 1981-2015 |
| **WRF-GCM** | Climate Change | UW Atmos. Sci. | CMIP5 (Table 2) | 13 | 1 hr | 12 km | 1970-2099 |

#### *Observationally-Based Historical Climate Dataset*

Past hydrologic studies have typically used interpolated estimates of daily weather on model grid cells (e.g., Hamlet et al. 2013). A novel aspect of the current approach is that we use dynamically downscaled historical meteorology, as is done for the climate change simulations. This has a number of advantages. First, we are able to use hourly meteorology as opposed to daily; a significant improvement given that instantaneous flows – the basis for many regulations and design standards – are not well correlated with daily-average flows, whereas the correlation is high for hourly flows. Second, regional models have been shown to better represent spatial variations in weather variables, particularly in complex topography or where observations are sparse. Finally, by using the same regional climate

model for both the historical and climate change simulations, we ensure that the hydrologic model is better adapted to accurately reflect the implications of climate change for hydrology.

For the historical dataset we used an implementation of WRF developed by Ruby Leung and colleagues at the Pacific Northwest National Laboratory (PNNL; hereafter, we refer to the historical WRF simulation as "WRF-OBS"). The dataset is produced using WRF version 3.2, with a model domain covering all of the western U.S., at an hourly time step and a spatial resolution of 6 km (Chen et al. 2018). Boundary conditions are taken from the North American Regional Reanalysis (NARR; Mesinger et al. 2006), and the simulation spans the years 1981-2015. Reanalysis datasets are essentially internally-consistent collections of weather observations; they are created by combining massive amounts of environmental observations in a Bayesian model framework that synthesizes them into the best estimate of the atmospheric state for each time step. NARR is produced for North America at a spatial resolution of 32 km.

*Future Climate Dataset*

A new ensemble of regional climate model projections was recently produced in collaboration with Cliff Mass in UW's department of Atmospheric Sciences (hereafter referred to as "WRF-GCM"). GCM projections were obtained from the Climate Model Inter-comparison Project, phase 5 (CMIP5; Taylor et al. 2012). GCMs were primarily selected based on Brewer et al. (2016), who evaluated and ranked global climate models based on their ability to reproduce the climate of the Pacific Northwest. The new ensemble of WRF projections includes one simulation for each of the GCMs listed in Table 2. All of the new projections are based on the high-end Representative Concentration Pathway (RCP) 8.5 scenario (Van Vuuren et al. 2011), with the exception of the ACCESS 1.0 GCM, for which an additional simulation was also produced for the low-end RCP 4.5 scenario. Simulations were performed using WRF version 3.2, implemented following Salathé et al. (2010, 2014). The innermost domain, at 12-km resolution, encompasses the U.S. Pacific Northwest. Simulations span the years 1970-2099 at an hourly time step. The model, and model configuration, are described in detail in Lorente-Plazas et al. (2018) and Mauger et al. (2018). In addition, Mauger et al. (2019) discuss approaches for using RCP 8.5 projections as an analog for what might be projected for the RCP 4.5 scenario. For example, temperature

**Table 2.** The twelve global climate models (GCMs) used as input to the regional model simulations. Horizontal resolution is given in degrees latitude × degrees longitude; "Vertical Levels" refers to the number of layers in the atmosphere model for each GCM. All simulations are based on the high-end RCP 8.5 greenhouse gas scenario (Van Vuuren et al. 2011). A low-end scenario was also produced for the ACCESS 1.0 model, resulting in two separate projections for this GCM.

| Model | Center | Resolution | Vertical Levels |
|---|---|---|---|
| **ACCESS1-0** | Commonwealth Scientific and Industrial Research Organization (CSIRO), Australia/ Bureau of Meteorology, Australia | 1.25° × 1.88° | 38 |
| **ACCESS1-3** | Commonwealth Scientific and Industrial Research Organization (CSIRO), Australia/ Bureau of Meteorology, Australia | 1.25° × 1.88° | 38 |
| **bcc-csm1-1** | Beijing Climate Center (BCC), China Meteorological Administration | 2.8° × 2.8° | 26 |
| **CanESM2** | Canadian Centre for Climate Modeling and Analysis | 2.8° × 2.8° | 35 |
| **CCSM4** | National Center of Atmospheric Research (NCAR), USA | 1.25° × 0.94° | 26 |
| **CSIRO-Mk3-6-0** | Commonwealth Scientific and Industrial Research Organization (CSIRO) / Queensland Climate Change Centre of Excellence, Australia | 1.8° × 1.8° | 18 |
| **FGOALS-g2** | LASG, Institute of Atmospheric Physics, Chinese Academy of Sciences | 2.8° × 2.8° | 26 |
| **GFDL-CM3** | NOAA Geophysical Fluid Dynamics Laboratory, USA | 2.5° × 2.0° | 48 |
| **GISS-E2-H** | NASA Goddard Institute for Space Studies, USA | 2.5° × 2.0° | 40 |
| **MIROC5** | Atmosphere and Ocean Research Institute (The University of Tokyo), National Institute for Environmental Studies, and Japan Agency for Marine-Earth Science and Technology | 1.4° × 1.4° | 40 |
| **MRI-CGCM3** | Meteorological Research Institute, Japan | 1.1° × 1.1° | 48 |
| **NorESM1-M** | Norwegian Climate Center, Norway | 2.5° × 1.9° | 26 |

changes for the 2080s in the RCP 4.5 projections appear to correspond approximately to the projections for the 2040s or 2050s in the RCP 8.5 projections.

**Table 3.** Weather stations used to evaluate WRF model biases.

| Source | ID | Name | Lat. | Lon. | Elv. (m) | Years |
|---|---|---|---|---|---|---|
| AWN | 330169 | Arlington | 48.2016 | -122.2262 | 10 | 2017-2019 |
| AWN | 330021 | Fir Island | 48.3565 | -122.4219 | 0 | 2008-2019 |
| AWN | 300214 | Langley | 48.0011 | -122.4328 | 51 | 2014-2019 |
| AWN | 330101 | Mt. Vernon | 48.4385 | -122.3857 | 7 | 1993-2019 |
| AWN | 330159 | Sakuma | 48.4974 | -122.3785 | 9 | 2006-2019 |
| AWN | 330092 | Seattle | 47.6570 | -122.2891 | 9 | 2011-2019 |
| AWN | 330162 | Snohomish | 47.9027 | -122.1147 | 0 | 2006-2019 |
| AWN | 330026 | Woodinville | 47.7484 | -122.1542 | 14 | 2008-2019 |
| GHCND | USC00450257 | Arlington | 48.2006 | -122.1281 | 31 | 1922-2019 |
| GHCND | USC00450456 | Baring | 47.7722 | -121.4819 | 235 | 1970-2019 |
| GHCND | USC00451233 | Cedar Lake HCN | 47.4144 | -121.7561 | 476 | 1898-2019 |
| GHCND | USC00451992 | Darrington RS | 48.2600 | -121.6036 | 168 | 1911-2019 |
| GHCND | USC00452675 | Everett HCN | 47.9753 | -122.195 | 18 | 1894-2019 |
| GHCND | USW00024222 | Everett-Snohomish AP | 47.9078 | -122.2803 | 185 | 1948-2019 |
| GHCND | USR0000WFIN | Finney Cr WA | 48.4028 | -121.7903 | 579 | 1985-2019 |
| GHCND | USR0000WGOH | Gold Hill WA | 48.2000 | -121.5000 | 1036 | 1990-2019 |
| GHCND | USC00454169 | Kent | 47.4172 | -122.2433 | 9 | 1912-2019 |
| GHCND | USC00454486 | Landsburg | 47.3767 | -121.9614 | 163 | 1903-2019 |
| GHCND | USC00455525 | Monroe | 47.8453 | -121.9944 | 37 | 1929-2019 |
| GHCND | USC00455678 | Mt Vernon 3-WNW | 48.4403 | -122.3867 | 4 | 1956-2005 |
| GHCND | USC00456295 | Palmer 3-ESE | 47.3058 | -121.8514 | 280 | 1924-2019 |
| GHCND | USW00094248 | Renton Muni Ap | 47.4933 | -122.2144 | 9 | 1998-2019 |
| GHCND | USW00024234 | Seattle Boeing Fld | 47.5303 | -122.3008 | 6 | 1948-2019 |
| GHCND | USW00094290 | Seattle Sand Pt WSFO | 47.6872 | -122.2553 | 18 | 1986-2019 |
| GHCND | USW00024233 | Seattle-Tacoma Intl Ap (72793) | 47.4444 | -122.3139 | 113 | 1948-2019 |
| GHCND | USC00457507 | Sedro-Woolley HCN | 48.4958 | -122.2355 | 18 | 1896-2019 |
| GHCND | USC00457773 | Snoqualmie Falls HCN | 47.5414 | -121.8361 | 134 | 1898-2019 |
| GHCND | USC00458034 | Startup 1-E | 47.8664 | -121.7175 | 52 | 1924-2019 |
| GHCND | USC00458508 | Tolt S Fk RSVR | 47.7000 | -121.6908 | 610 | 1962-2019 |
| SNOTEL | 908 | Alpine Meadows | 47.78 | -121.70 | 1067 | 1994-2018 |
| SNOTEL | 898 | Mount Gardner | 47.36 | -121.57 | 890 | 1993-2018 |
| SNOTEL | 672 | Olallie Meadows | 47.37 | -121.44 | 1228 | 1980-2018 |
| SNOTEL | 911 | Rex River | 47.30 | -121.60 | 1161 | 1995-2018 |
| SNOTEL | 912 | Skookum Creek | 47.68 | -121.61 | 1009 | 1995-2018 |
| SNOTEL | 899 | Tinkham Creek | 47.33 | -121.47 | 911 | 1993-2018 |

## Climate Data Bias-Correction

Prior to calibrating the hydrologic model, we evaluated the historical WRF-OBS simulation to quantify its biases and determine how best to correct them to minimize the effect of these biases on the hydrologic simulations. We evaluated WRF in two different ways:

1. By comparing WRF with surface weather observations, and
2. By using WRF to simulate snowpack and comparing the results to observations.

Together these allowed us to identify key biases and correct for them prior to embarking on the hydrologic model calibration. Results from each are described in detail below.

### *Comparison with surface weather observations*

We compared the WRF-OBS results with surface observations from the 35 weather stations listed in Table 3. Observations were obtained from three sources:

1. GHCN-D (Global Historical Climate Network - Daily; Menne et al. 2012). This dataset includes daily observations of total precipitation, minimum temperature, and maximum temperature.
2. SNOTEL-BCQC (Snow Telemetry Bias Correction and Quality Control; Sun et al. 2019; Yan et al. 2018). This dataset includes daily observations of total precipitation, minimum temperature, and maximum temperature.
3. AWN (Ag Weather Net; http://weather.wsu.edu). This dataset includes hourly observations of precipitation, temperature, humidity, and shortwave radiation.

We compared these observations against results from the nearest grid cell from the WRF-OBS simulation. To account for elevation differences between WRF grid cells and the observations, we adjusted the observed temperatures based on an assumed lapse rate of 4.5ºC/km. Biases were calculated by comparing the full WRF-OBS simulation (1981-2015) with all valid observational data from 1970 to 2019, for each weather station. Our analysis included annual and seasonal averages as well as extreme metrics.

Figure 1 shows the comparison between the annual average of daily minimum and maximum temperatures. Although the biases are similar for the two maps, they differ substantially among stations and do not exhibit a clear geographic pattern. On average the comparisons suggest a slight cold bias in the WRF-OBS simulation. Figure 2 shows the comparison with annual precipitation and the top 1% of precipitation events in each year.

These show a much clearer pattern, relatively consistent among both metrics, of a dry bias in the WRF-OBS simulation.

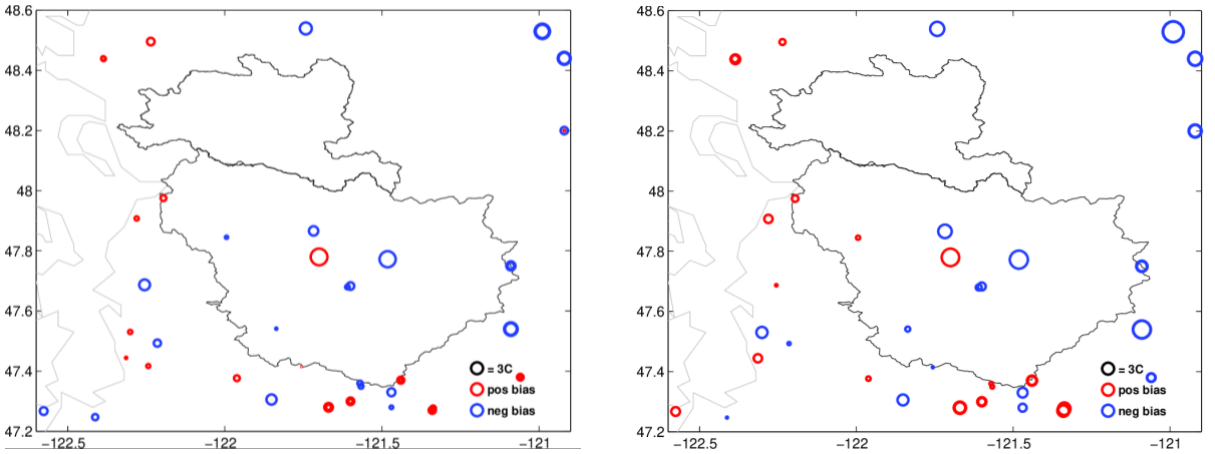


**Figure 1.** Map of the annual average temperature biases for the WRF-OBS simulation. The left-hand map shows the biased for the annual average of daily maximum temperatures, while the right-hand map shows the same for maximum temperatures. The size of each circle denotes the bias (°C), while the color denotes the sign of the bias. The Stillaguamish and Snohomish watersheds are outlined in black, while the Puget Sound coastline is shown in grey.

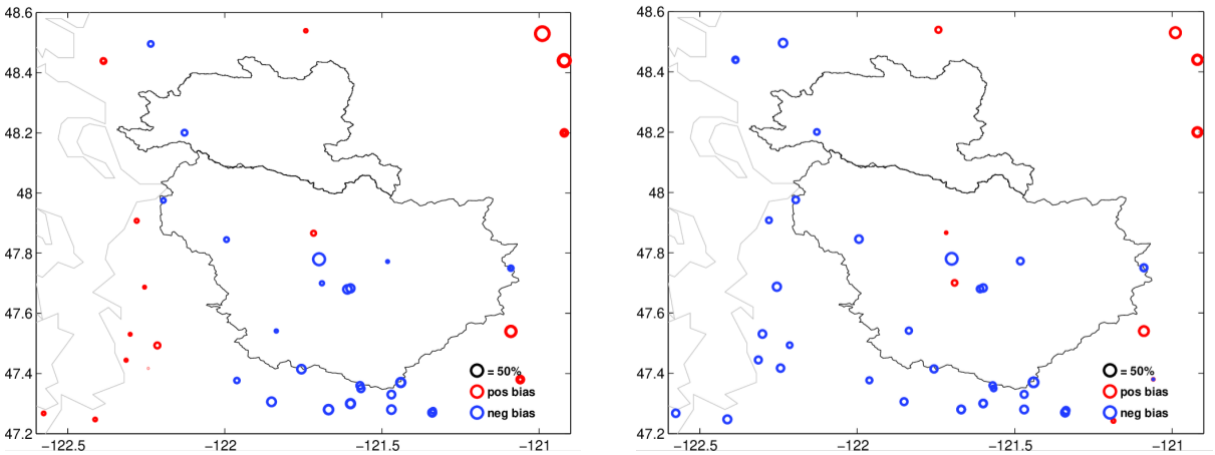


**Figure 2.** As in Figure 1 except showing the annual average (left) and top 1% (right) precipitation biases (%) for the WRF-OBS simulation.

Some weather stations included measurements of wind and shortwave radiation. Since these were available at fewer locations, Figure 3 shows the comparisons for the entire state of Washington. These showed a very consistent pattern of overestimating both wind speed and incoming shortwave radiation everywhere in the state.

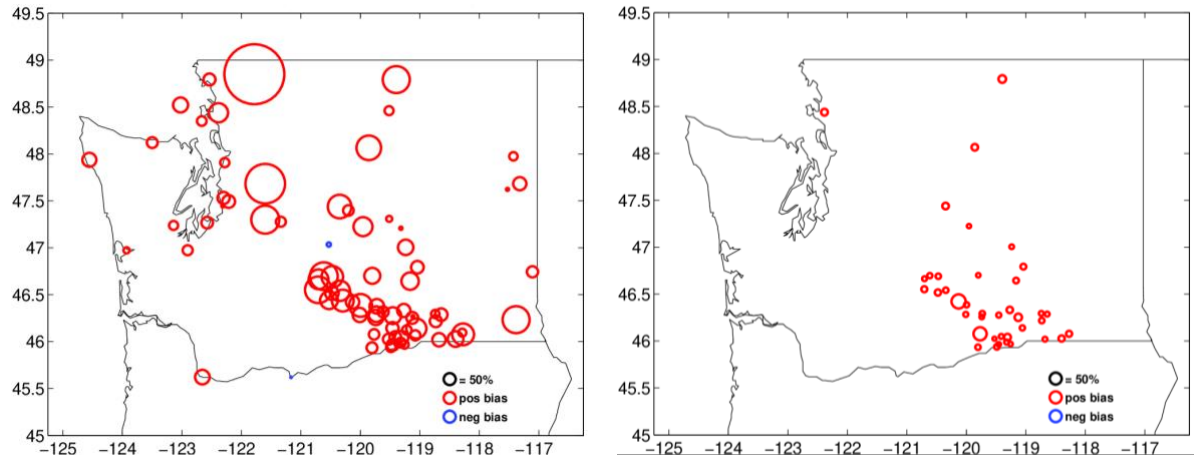


**Figure 3.** As in Figure 1 except showing the bias in annual average wind speed (left) and incoming shortwave radiation (right). Results are shown for the entire state of Washington since relatively fewer observations are available.

Based on these comparisons, we took a simplified approach to bias-correcting the WRF results, where we applied a uniform scaling based on the average bias among all comparisons across the two watersheds. We took the same approach for wind and shortwave radiation, while also comparing with the statewide average to ensure consistency given the relatively smaller number of stations available for comparison in the vicinity of the Stillaguamish and Snohomish watersheds. The bias corrections we applied to the WRF-OBS results are shown in Table 4.

**Table 4.** Bias-corrections applied to WRF-OBS results. These were applied uniformly to all grid cells and all time steps.

| Variable | Scaling |
|---|---|
| **Temperature** | +0.2°C |
| **Precipitation** | +15% |
| **Wind** | -40% |
| **Shortwave radiation** | -10% |

Humidity estimates from WRF were not bias-corrected. Although observations are available, tests indicated that adjustments to humidity could frequently lead to over-saturated air or other physically implausible conditions. Future work could

develop an improved approach, in which the relative humidity is corrected, then converted to vapor pressure deficit as used by the hydrologic model. Regardless of the approach, adjustments to humidity are unlikely to have a large effect on flood peaks.

No observational comparisons were made for longwave radiation because very few observations exist. Instead, longwave estimates were estimated using an empirical formulation (Dilly and O'Brien, 1998; Unsworth and Monteith, 1975), which previous research suggests is superior to WRF longwave estimates (Currier et al. 2017).

## Hydrologic Model

We modeled the hydrology of the two watersheds using the Distributed Hydrology Soil Vegetation Model (DHSVM; Wigmosta et al. 1994). DHSVM is an open-source model maintained by PNNL (http://dhsvm.pnnl.gov/). DHSVM has been widely applied in the mountainous western United States (e.g., Storck et al. 1998, Bowling and Lettenmaier 2001, Whitaker et al. 2003) and used to assess the impacts of climate change (e.g., Elsner et al. 2010, Vano et al. 2010, Cuo et al. 2011, Dickerson-Lange and Mitchell 2013, Cristea et al.

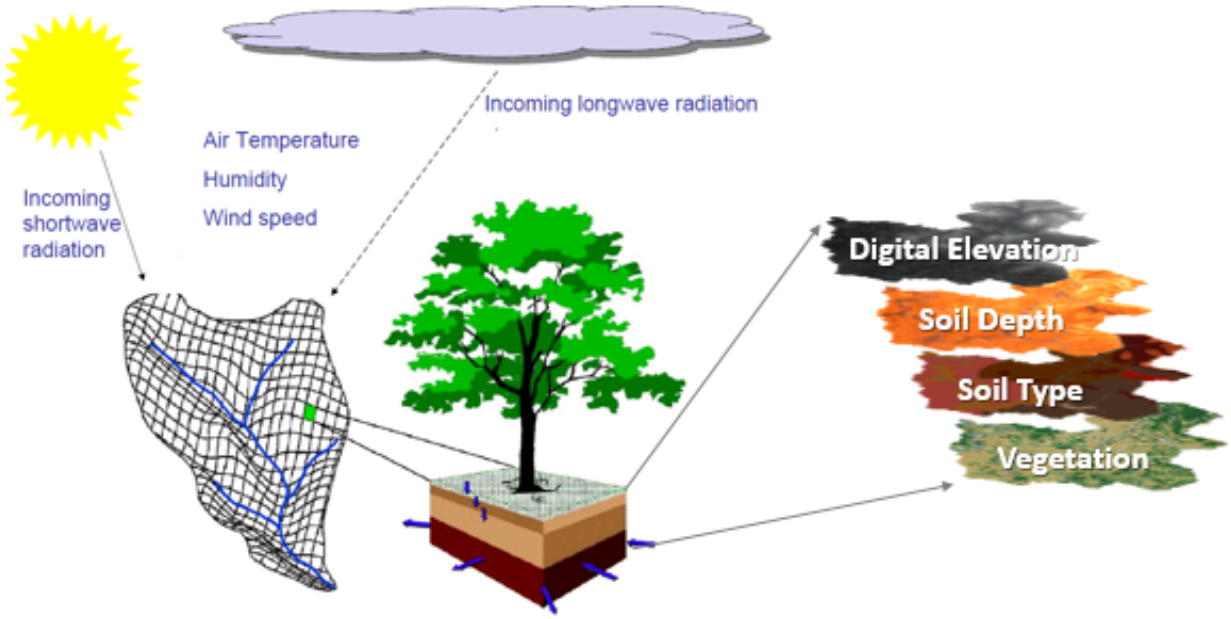


**Figure 4.** Diagram of DHSVM model and its inputs.

2014, Naz et al. 2014, Mauger et al. 2016) and land use (e.g., Sun et al. 2013, Cuo et al. 2009, 2011) on streamflow.

The DHSVM is a physically-based, spatially-distributed hydrological model that accounts for physical processes affecting the distribution of precipitation, partitioning of rain vs. snow, and tracking the movement of water on and through landscapes. The model represents the spatial distribution of evapotranspiration, snow cover, soil infiltration and moisture, and runoff across a watershed in a distributed fashion, requiring model inputs of geographic and climate information (Wigmosta et al. 2002; Figure 4). The model simulates one or more unsaturated soil layers and a saturated bottom layer. Subsurface flow in the saturated zone is based on a quasi-equilibrium approach described by Wigmosta and Lettenmaier (1999). The DHSVM represents snow accumulation and melt by calculating the full surface energy balance independently at each model grid cell, accounting for terrain shading effects, radiation attenuation, wind modification and snow-canopy processes (Wigmosta et al. 1994, Storck 2000, Storck et al. 2002, Andreadis et al. 2009, Sun et al. 2018, Sun et al. 2019). Prior research has shown that DHSVM snow simulations are sensitive to the choice of both incoming shortwave and longwave radiation, with melt initiation and rate more sensitive to longwave than shortwave radiation (Hinkelman et al. 2015). Stream channel routing is performed using a storage accounting scheme, which allows the user to produce hydrographs at any location along the channel network. Typical spatial resolution of DHSVM implementations range from about 10 m to 200 m.

*Meteorological Inputs*

Six meteorological variables are required to force the DHSVM simulations: temperature (°C), relative humidity (%), precipitation (m), wind speed (m/s), incoming shortwave radiation ($W/m^2$), and incoming longwave radiation ($W/m^2$). Meteorological inputs for DHSVM were created by simply applying the corrections in Table 4 uniformly to each time step, for each WRF-OBS grid cell in the model domains.

The WRF-GCM inputs for DHSVM were created by first interpolating them from their native 12-km grid to the 6 km WRF-OBS grid, using a bi-linear interpolation. We then compared the historical average (1981-2015) for each model simulation against the average over the same time period in the bias-corrected WRF-OBS results. This comparison provided the bias-correction factors to be applied to each WRF-GCM simulation, which were then used to

create the DHSVM inputs for that simulation. Longwave was then recomputed using the same empirical formulation described above (Dilly and O'Brien, 1998; Unsworth and Monteith, 1975).

*Model Setup*

For this study we used DHSVM version 3.2, which includes a number of updates, most notably a new canopy gap component with enhanced radiation transmittance schemes and physical processes controlling snowpack evolution in forest gaps (Sun et al. 2018,

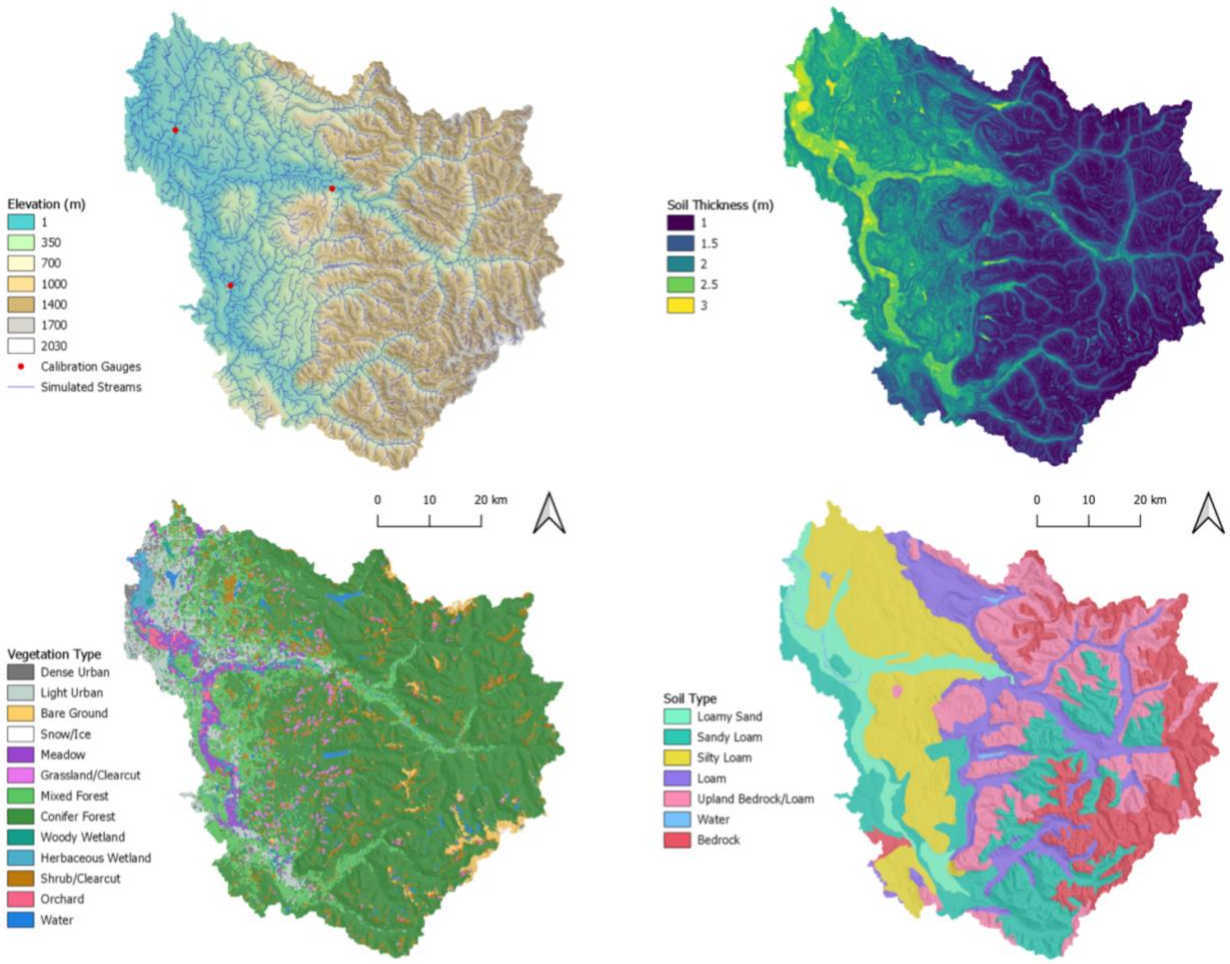


**Figure 5.** Maps showing the DHSVM DEM, vegetation, and soil characteristics for the Snohomish model.

https://github.com/pnnl/DHSVM-PNNL). We implemented the model at a resolution of 150 m, after testing suggested that finer resolutions resulted in peak flow hydrographs that were unrealistically muted or delayed since flow from grid cell to grid cell can only move across one cell boundary per time step (Dubin and Lettenmaier, 1999). We used a 1-hour time step for improved resolution of peak flows.

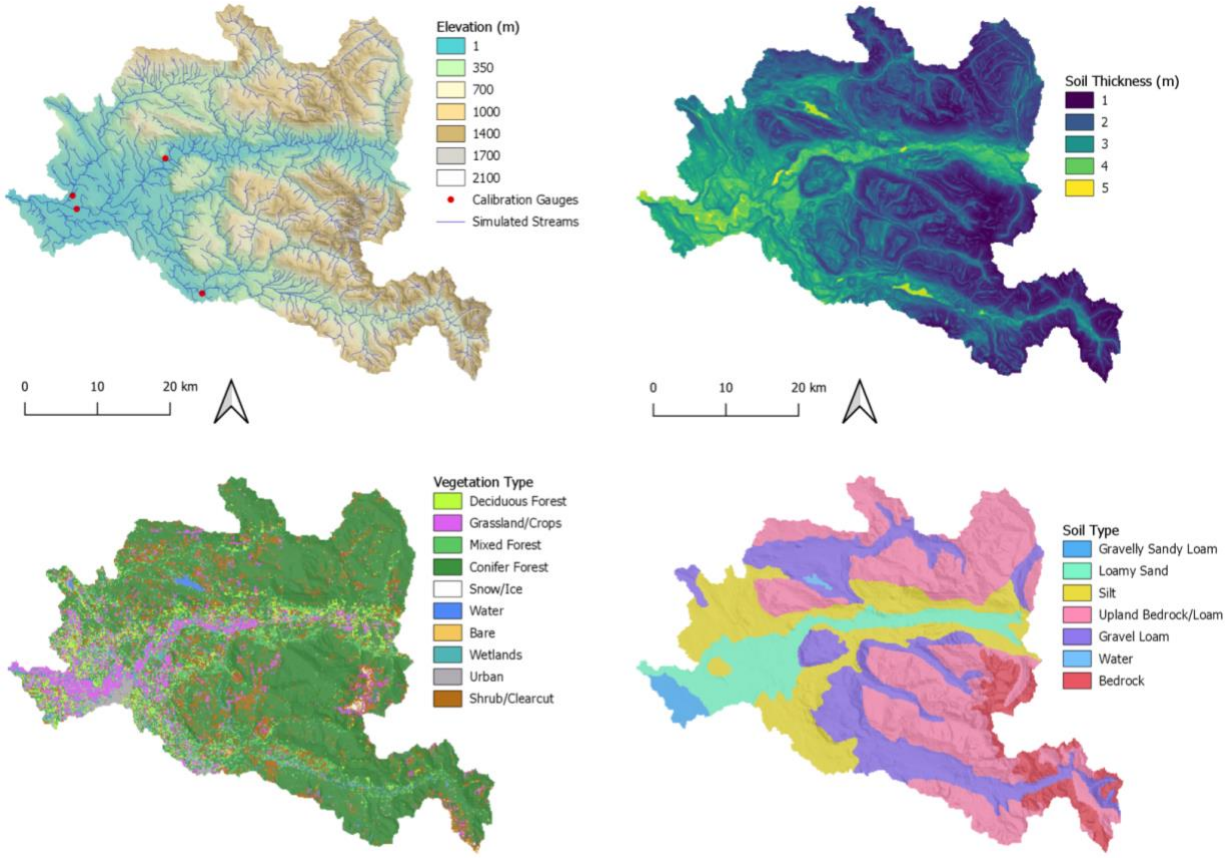


**Figure 6.** As in Figure 5 but for the Stillaguamish model.

*Topography and Stream Network*

The digital elevation models (DEM) were downloaded from the National Elevation Dataset[1]

[1] http://viewer.nationalmap.gov/basic/

(Elevation products, 3DEP) for the Snohomish model and from the Washington State GIS server[2] for the Stillaguamish model. The DEM (top left panel in Figures 5 and 6) provides a base layer of spatial information and is used to generate watershed boundaries using ArcGIS hydrology modeling tools. DHSVM-PNNL Python scripts that drive ArcGIS tools are used to develop a stream network based on a user-defined contributing area. Simulated streamflows are routed through the stream network based on flow direction relationships from upgradient (higher elevation) to downgradient (lower elevation) grid cells and stream channel segments.

*Land Cover*

We generated the Snohomish land cover grids based on the National Land Cover Database 2016 update (NLCD; Homer et al. 2020, Jin et al. 2019, Yang et al. 2018). This is the most recent national land cover product, with a 16-class land cover classification scheme applied at a spatial resolution of 30 meters based on Landsat satellite data and created by the Multi-Resolution Land Characteristics Consortium (Homer et al. 2015). For the Stillaguamish, land cover grids were based on the Coastal Change Analysis Program (C-CAP; NOAA, 2019); results should be the same as those obtained from NLCD. For both basins, land cover grids were resampled to 150 m resolution. Land cover is dominated by evergreen forest in the upper elevations while the lower elevations are more developed with urban and agricultural classifications (Table 5; bottom left panel in Figures 5 and 6).

**Table 5.** Land cover classifications used as input to the DHSVM model.

| ID | NLCD IDs | Land Cover Type |
|---|---|---|
| 1 | 23, 24 | Dense Urban (>75%) |
| 2 | 21, 22 | Light / Medium Urban (<75%) |
| 3 | 31 | Bare Ground |
| 4 | 12 | Snow / Ice |
| 5 | 81 | Hay / Pasture |
| 6 | 71 | Grassland/Herbaceous |
| 7 | 41, 43 | Mixed / Deciduous Forest |
| 8 | 42 | Conifer Forest |
| 9 | 90 | Woody Wetlands |
| 10 | 95 | Emergent Herbaceous Wetl. |
| 11 | 52 | Shrub / Scrub |
| 12 | 82 | Orchard |
| 13 | 11 | Water |

[2] http://gis.ess.washington.edu/data/raster/tenmeter/byquad/index.html

### *Soil Parameters*

The Digital General Soil Map of the United States, or STATSGO dataset (NRCS 2017) was developed for regional and national studies designed for broad planning and management uses requiring estimates of soil characteristics. The soil units are distributed as spatial and tabular datasets with 1-kilometer resolution for the conterminous United States. In our study areas, the STATSGO database contained seven different soil map units in each watershed from which DHSVM soil parameters can be derived. Silt and loam units make up the majority of both basins (bottom right panel in Figures 5 and 6).

### *Soil Depth*

Soil depths are defined empirically based on elevation and local slope using DHSVM-PNNL Python scripts[3]. The algorithm generates thin soils on steep slopes and ridge tops and thick soils on gentle slopes and in depressions, within a user-defined defined range (1.0 – 3.0 m for the Snohomish model and 1.0 – 5.0 m for the Stillaguamish model; top right panel in Figures 5 and 6).

## Calibration

### *Snohomish Model Calibration*

Initial model testing consisted of comparing snow simulations to Snowpack Telemetry (SNOTEL) observations within the area (Table 6, example comparisons in Figure 7). We performed point simulations at each location, comparing the timing and magnitude of snow simulations against observations. This is a good test of the climate forcings, as well as the snow/rain threshold temperatures and the temperature lapse rates in the DHSVM model. Although a precipitation lapse rate can also be specified in DHSVM, this was not included since

**Table 6.** Snowpack Telemetry (SNOTEL) sites used to evaluate the Snohomish DHSVM snow simulations.

| *SNOTEL Site* | *ID* | *Lat. / Lon.* | *Elv (m)* | *Years* |
|---|---|---|---|---|
| **Skookum Creek** | 912 | 47.68N / 121.61W | 1009 | 1995-2018 |
| **Alpine Meadows** | 908 | 47.78N / 121.7W | 1067 | 1994-2018 |
| **Stevens Pass** | 191 | 47.75N / 121.09W | 1204 | 1980-2018 |

[3] https://github.com/pnnl/DHSVM-PNNL

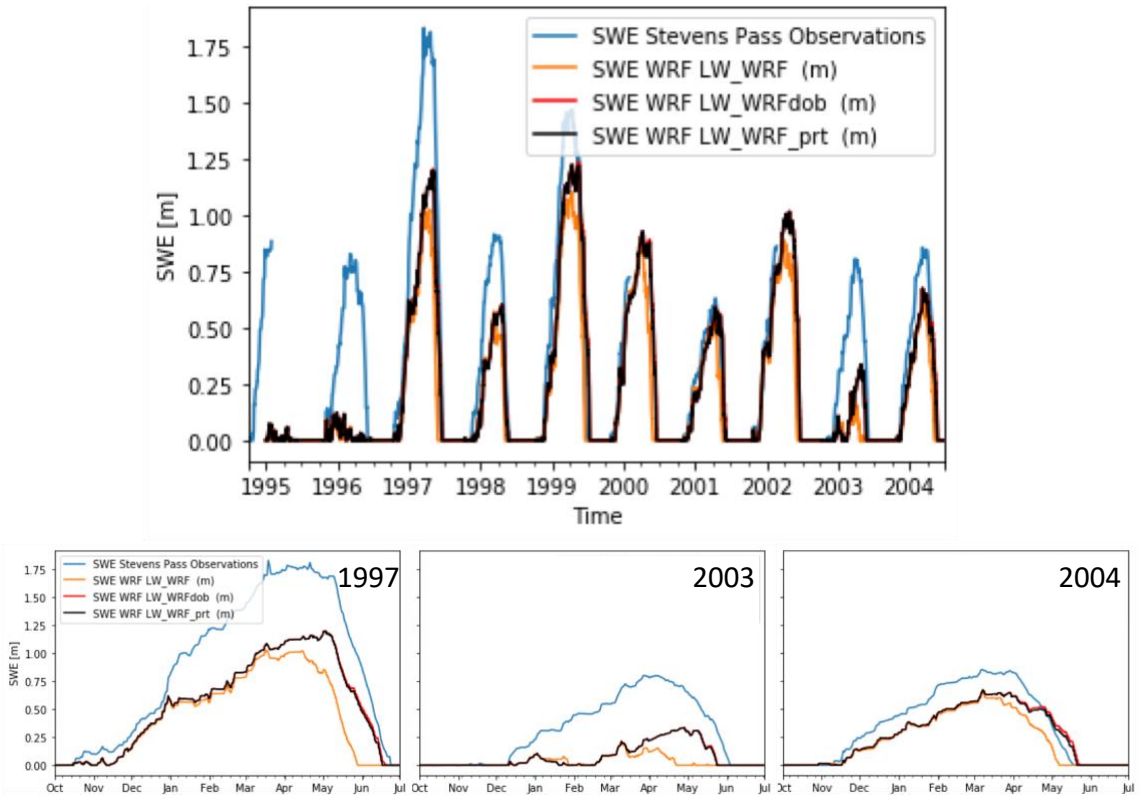


**Figure 7.** Example showing comparisons of snow water equivalent (SWE) among different longwave schemes for the Stevens Pass station. The longwave schemes include the estimates obtained directly from the WRF-OBS simulation, as well as the empirical approaches of Dilly and O'Brien (1998; "dob") and Prata (1996; "prt"). These show that all estimates cause the snow to melt earlier than the observations, but that the WRF longwave estimates have the largest biases and there is very little difference among the two empirical approaches.

the dynamically-downscaled projections already provide physically-based estimates of the spatial distribution in precipitation.

For the comparisons we chose contrasting years: 1997 was particularly wet, 2003 relatively dry, and 2004 was representative of normal conditions. The results largely confirmed our existing WRF-OBS bias

**Table 7.** DHSVM global lapse rates and snow/rain thresholds used in the Snohomish.

| Parameter | Value |
|---|---|
| Temperature Lapse Rate | -4.5°C/km |
| Precipitation Lapse Rate | 0.0 m/km |
| Snow Threshold | -1.0 °C |
| Rain Threshold | +0.5 °C |

**Table 8.** Streamflow sites used in this study; the three calibration sites are highlighted in bold. The table lists the water years (Oct-Sep) of quality-controlled observations that overlap with the years in the WRF-OBS simulation, and notes if observed flows are regulated or not ("Dam?"). Flows at two sites are affected by the SF Tolt Reservoir.

| *Site Name* | *USGS ID* | *Water Years* | *Dam?* |
|---|---|---|---|
| SF Snoqualmie R. at North Bend | 12144000 | 1981-2015 | N |
| MF Snoqualmie R. near Tanner | 12141300 | 1981-2015 | N |
| NF Snoqualmie R. near Snoqualmie Falls | 12142000 | 1981-2015 | N |
| Snoqualmie R. near Snoqualmie | 12144500 | 1981-2015 | N |
| Raging R. near Fall City | 12145500 | 1981-2015 | N |
| NF Tolt R. near Carnation | 12147500 | 1981-2015 | N |
| **Snoqualmie R. near Carnation** | **12149000** | **1981-2015** | **Y** |
| **Skykomish R. near Gold Bar** | **12134500** | **1981-2015** | **N** |
| Snohomish R. near Monroe | 12150800 | 1981-2015 | Y |
| **Pilchuck R. near Snohomish** | **12155300** | **1992-2015** | **N** |

correction while also leading us to refine the temperature lapse rate used to account for the elevation differences between the WRF grid cell and each DHSVM grid cell (Table 7).

We then performed a streamflow calibration using a multi-objective complex evolution global optimization method (MOCOM-UA) which was developed by the Land Surface Hydrology group at the University of Washington, following the approach of Yapo et al. (1998). The objective of the model calibration was to maximize the Nash-Sutcliffe efficiency (NSE) and Kling-Gupta efficiency (KGE) coefficients (Nash and Sutcliffe 1970, Gupta et al. 2009) between observed and simulated daily mean streamflow and log-transformed daily streamflow. We calibrated the model to streamflow observations at the three gauges highlighted in Table 8. To ensure that these

**Table 9.** Parameters and soil types used in the calibration.

| Parameter | Range | Soil Type | Final |
|---|---|---|---|
| **Lateral Conductivity** | 0.0000002 – 0.02 | Sandy Loam | 0.0145 |
| | | Silty Loam | 0.0178 |
| **Exponential Decrease** | 1 – 3 | Sandy Loam | 1.87 |
| | | Silty Loam | 1.15 |

results are representative across the watershed we verified the results at the other gauges listed in Table 8.

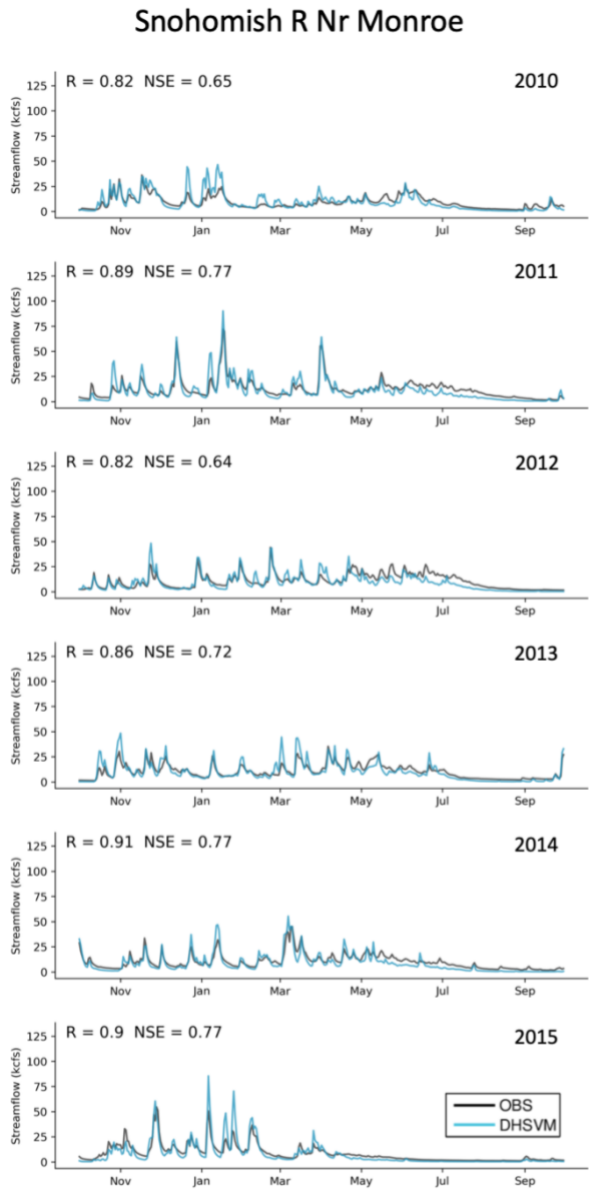


**Figure 8.** Observed and modeled daily flows for the Snohomish River Near Monroe (USGS ID: 12150800). Results are shown for water years 2010-2015; comparisons for other years are similar.

We performed sensitivity tests, identifying parameters such as lateral saturated conductivity (m/s) and exponential decrease for sandy loam (one of the major soil types that could be adjusted to improve the match between simulated and observed streamflow. We used ranges for each parameter value based on the published literature (Table 9).

Comparisons between observed and calibrated daily flows are shown in Figure 8; model skill scores are shown in Table 10. Other sites that were not used to calibrate DHSVM are also included in the tables, which show good agreement between the

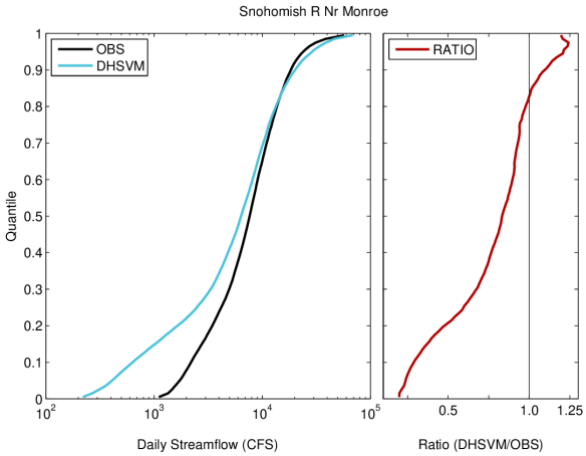


**Figure 9.** Observed and modeled cumulative distribution functions (CDFs, or flow duration curves; left), and their ratio (DHSVM/observations, right), for the Snohomish River Near Monroe.

simulation and observations (daily r >= 0.76 and NSE >= 0.56).

In order to evaluate the model as a function of flow quantile, Figure 9 shows a comparison of the cumulative distribution functions (CDFs), for observed and simulated daily flows for the Snohomish River Near Monroe. We used daily mean flows for this comparison since these receive more thorough quality control than the sub-daily flows that are provided by USGS. This shows that the model does a decent job of capturing high flows but is much too low relative to observed low flows. Given our focus on peak flows we consider this adequate for the current project. In addition, since our focus is on the sensitivity to climate change – as opposed to precise estimates of absolute flows – the high correlations noted in Table 10 indicate that the model is sufficiently well calibrated for the purposes of the current study.

**Table 10.** Model evaluation scores for Snohomish DHSVM. Model results were compared to observations using the correlation (r), Nash-Sutcliffe Efficiency (NSE), and Kling-Gupta Efficiency (KGE), for daily, monthly, and water year peak flows. The "Water Years" column lists the years for which there is overlap between the observations and the historical simulation.

| | Water Years | Daily | | | Monthly | | |
|---|---|---|---|---|---|---|---|
| **Site Name** | | **r** | **NSE** | **KGE** | **r** | **NSE** | **KGE** |
| SF Snoqualmie R. at North Bend | 1981-2015 | 0.83 | 0.66 | 0.81 | 0.86 | 0.72 | 0.82 |
| MF Snoqualmie R. near Tanner | 1981-2015 | 0.85 | 0.70 | 0.82 | 0.88 | 0.73 | 0.84 |
| NF Snoqualmie R. near Snoq. Falls | 1981-2015 | 0.82 | 0.64 | 0.76 | 0.89 | 0.72 | 0.80 |
| Snoqualmie R. near Snoqualmie | 1981-2015 | 0.85 | 0.70 | 0.82 | 0.88 | 0.76 | 0.83 |
| Raging R. near Fall City | 1981-2015 | 0.81 | 0.59 | 0.79 | 0.90 | 0.80 | 0.89 |
| NF Tolt R. near Carnation | 1981-2015 | 0.80 | 0.56 | 0.57 | 0.89 | 0.50 | 0.61 |
| Snoqualmie R. near Carnation | 1981-2015 | 0.85 | 0.72 | 0.82 | 0.89 | 0.79 | 0.83 |
| Skykomish R. near Gold Bar | 1981-2015 | 0.78 | 0.61 | 0.68 | 0.84 | 0.69 | 0.84 |
| Snohomish R. near Monroe | 1981-2015 | 0.86 | 0.74 | 0.75 | 0.88 | 0.77 | 0.83 |
| Pilchuck R. near Snohomish | 1992-2015 | 0.76 | 0.47 | 0.72 | 0.89 | 0.74 | 0.82 |

*Stillaguamish Model Calibration*

There are no SNOTEL stations within the Stillaguamish watershed. As a consequence, we relied on watershed-adjacent NRCS SNOTEL stations (Table 6) and observed historical streamflow to calibrate the Stillaguamish model. Our baseline parameterization started from prior DHSVM-based studies in the North and South Forks of the Stillaguamish (Freeman, 2019; Clarke, 2020). From there we iteratively altered meteorology, soil, snow, and vegetation parameters in a manner similar to that described above for the Snohomish watershed.

**Table 11.** Lapse rates and rain/snow thresholds used for the Stillaguamish model

| Parameter | | Value |
|---|---|---|
| Monthly Temperature Lapse Rate | Oct | -4.5°C/km |
| | Nov-Mar | -5.5°C/km |
| | Apr | -5.0°C/km |
| | May | -4.5°C/km |
| | Jun-Sep | -4.0°C/km |
| Precipitation Lapse Rate | | 0.0 m/km |
| Snow Threshold | | +1.0 °C |
| Rain Threshold | | +1.0 °C |

Parameterizing meteorological constants within DHSVM proved to be the most challenging aspect for the Stillaguamish DHSVM calibration. The goal for meteorological calibration was to produce model estimates of snow water equivalent (SWE) that were similar to those observed at the Skookum Creek and Alpine Meadows NRCS SNOTEL stations within elevation bands (i.e., 1005 -1070 m) similar to the Stillaguamish watershed. Although they are located outside of the Stillaguamish watershed (within 100 km), we considered these to be a proxy for conditions in the Stillaguamish watershed given their similar geographic settings. We achieved a qualitatively satisfactory SWE calibration using the seasonal temperature lapse rates and snow and rain temperature thresholds shown in Table 11.

Generally, the Stillaguamish model produced less SWE with this parameterization than what was observed at the Skookum Creek and Alpine Meadows SNOTEL stations (Figure 10); however, SWE can vary over similar geographies and altitudes due to unique alpine microclimates, so this bias may be inconsequential or simply a limitation of model resolution. We selected our seasonal lapse rates based on iterative testing and literature values for similar watersheds (Minder et al. 2010). We were able to improve peak April 1 SWE and spring freshet using higher temperature lapse rates in winter months (to produce

colder temps at higher elevations) and lower temperature lapse rates in late spring/summer months (to promote snowmelt in late spring/early summer).

We evaluated model skill at four gauging sites in different tributaries of the Stillaguamish (Table 12), focusing our calibration on model performance at the Stillaguamish River Near Silvana site. Based on these comparisons, we calibrated the soil parameters for the Stillaguamish through manual iterative statistical analysis, using MOCOM-UA on select highly sensitive parameters. The objective of our calibration was to maximize KGE and NSE between observed and simulated daily streamflows while minimizing percent bias.

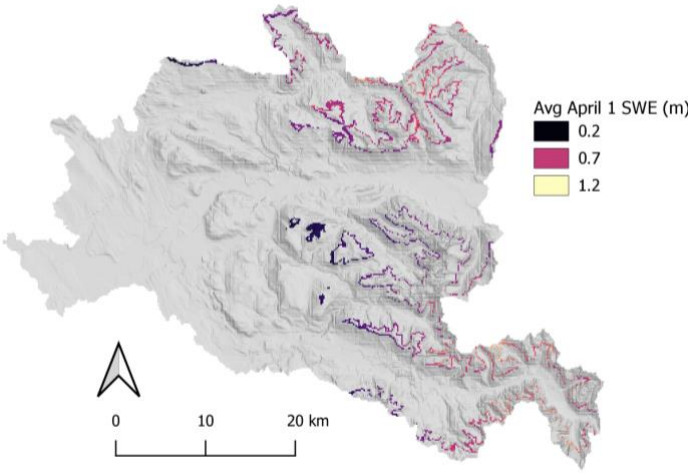


**Figure 10.** Map of average April 1st simulated SWE for water years 2004 through 2015 for pixels with elevations between 1005 and 1070 meters above sea level. This elevation band comprises the elevations of the Skookum Creek and Alpine Meadows SNOTEL stations in the adjacent Snohomish basin (Table 6). Average simulated SWE for these pixels was 0.6 meters; average observed SWE at the Skookum Creek and Alpine meadows stations was 1.07 m.

**Table 12.** Streamflow observations that were used in evaluating the Stillaguamish model; the calibration site is highlighted in bold. The table lists the water years (Oct-Sep) of quality-controlled observations that overlap with the years in the WRF-OBS simulation. There are no dams within the Stillaguamish Watershed.

| *Site Name* | *Source* | *ID* | *Water Years* |
|---|---|---|---|
| **Stillaguamish R near Silvana (I-5 Bridge)** | **Ecology** | **05A070** | **2011-2015** |
| NF Stillaguamish River near Arlington | USGS | 12167000 | 2004-2015 |
| S.F. Stillaguamish R. at Jordan Rd. Bridge | Ecology | 05A105 | 2004-2015 |
| Pilchuck Cr. at Bridge 626 | Ecology | 05D070 | 2004-2015 |

The most sensitive soil parameters in the Stillaguamish were lateral conductivity, exponential decrease, and porosity of the major soil units in the watershed (Upland Bedrock/Loam, Gravel Loam, and Silt; Figure 6). Field capacity was also highly sensitive but generally related to porosity for each unit (i.e., when porosity was greater, field capacity was also greater). Compared to literature values (e.g., Du et al. 2014, Beckers et al. 2004, Freeman 2019, Clarke 2020), our calibrated soil porosities are low; however, this is likely a function of the goals of our research: to produce a model skilled at producing accurate peak flows.

**Table 13.** Select parameterization changes from baseline to final calibration for the Stillaguamish DHSVM model.

| ***Parameterization*** | | ***Baseline*** | ***Final*** |
|---|---|---|---|
| Soils | | | |
| Upland Bedrock/ Loam | Lateral Conductivity | 0.0001 m/s | 0.0002 m/s |
| | Exponential Decrease | 2.3 | 1.6 |
| | Porosity (three layers) | 0.3 / 0.3 / 0.3 | 0.26 / 0.25 / 0.25 |
| Gravel Loam | Lateral Conductivity | 0.0005 m/s | 0.008 m/s |
| | Exponential Decrease | 3 | 0.6 |
| | Porosity (three layers) | 0.45 / 0.45 / 0.45 | 0.26 / 0.23 / 0.23 |
| Vegetation | | | |
| Rain/Snow LAI Multipliers | | 0.0003 / 0.0003 | 0.0001 / 0.0003 |
| Conifer Forests | Overstory LAI | 12 | 8 |
| | Understory LAI | 3 | 0.2 |

Vegetation parameters were generally less sensitive than meteorological or soil parameters in the Stillaguamish; however, we did perform some iterative sensitivity testing and parameterization of overstory leaf area index (LAI) and LAI multipliers for coniferous forests (the dominant landcover unit in the watershed). Select parameterization changes from baseline through calibration are shown in Table 13. Unlike in the Snohomish model, we did not use the variable light transmittance functionality of DHSVM version 3.2.

Comparisons between the observed and simulated daily time series and CDFs are shown in Figures 11 and 12, respectively; model evaluation scores are shown in Table 14.

**Table 14.** Model evaluation scores for the calibrated Stillaguamish DHSVM WRF-OBS model.

| Site Name | Water Years | Daily | | | Monthly | | |
|---|---|---|---|---|---|---|---|
| | | r | NSE | KGE | r | NSE | KGE |
| Stillaguamish R near Silvana (I-5 Bridge) | 2010-2014 | 0.79 | 0.59 | 0.76 | 0.90 | 0.78 | 0.81 |
| NF Stillaguamish R nr Arlington | 2005-2014 | 0.79 | 0.57 | 0.76 | 0.87 | 0.72 | 0.80 |
| SF Stillaguamish R. at Jordan Rd. Bridge | 2005-2014 | 0.81 | 0.61 | 0.70 | 0.89 | 0.67 | 0.71 |
| Pilchuck Cr. at Bridge 626 | 2005-2014 | 0.75 | 0.56 | 0.64 | 0.87 | 0.76 | 0.78 |

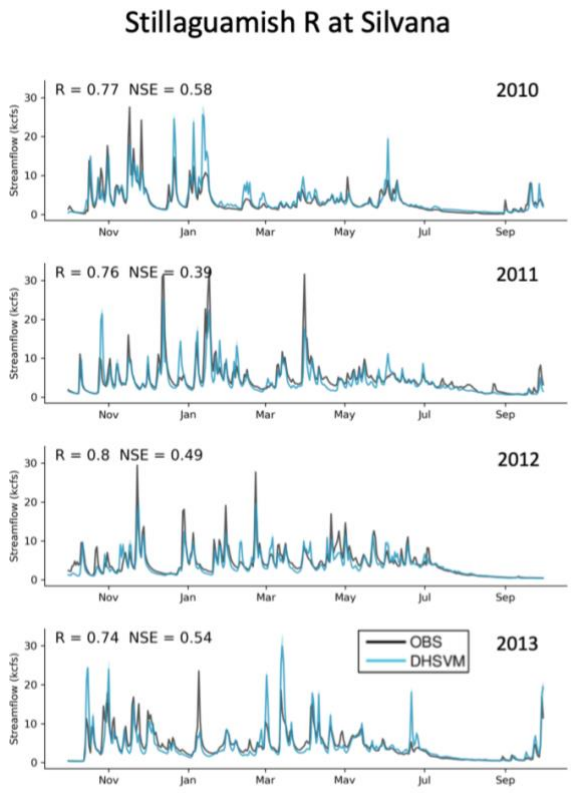


**Figure 11.** Observed and modeled daily flows at for the Stillaguamish River at Silvana (Ecology 05A070). Results are shown for water years 2010 through 2013.

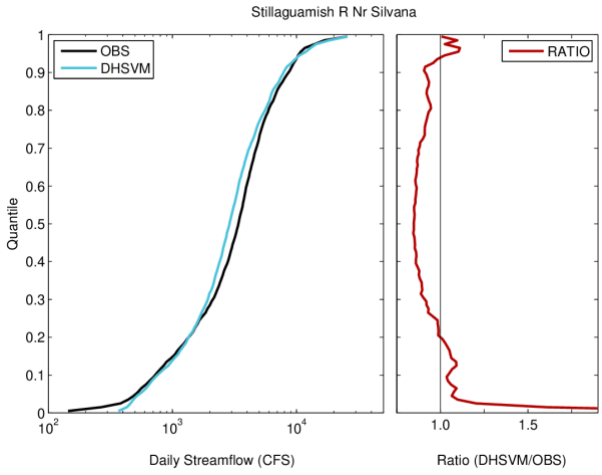


**Figure 12.** Observed and modeled cumulative distribution functions (CDFs, or flow duration curves; left), and their ratio (DHSVM/observations, right), for the Stillaguamish River Near Silvana.

## Post-Processing and Analysis

The historical DHSVM simulation, using the WRF-OBS inputs, runs from 1981-2015. The climate change simulations, based on the 13 WRF-GCM projections (Tables 1 and 2), run from 1970-2099. Focusing on the WRF-GCM simulations, this section describes how the results were processed to assess changes, with a particular focus on peak flows.

### *Peak Flow Statistics*

We computed extreme statistics using water year peak flow maxima, for multiple flow durations: 1-hour, 1-day, 3-day, and 7-day. To calculate extreme statistics (e.g., 10-year event, 1-day duration), we used L-moments to fit generalized-extreme value (GEV) distributions to simulated annual peak flows, following the methodology described in Salathé et al. (2014) and Tohver et al. (2014). Previous studies indicate that GEV distributions are superior to Log-Pearson Type 3 distributions – the standard flood frequency analysis method used by the USGS (Rahman et al. 1999 & 2015, Vogel et al. 1993, Nick et al. 2011). We used a bootstrap approach to construct our GEV distributions by resampling 1,000 times, with replacement, from each historical and future time period.

### *A Focus on the Relative Change in Flow*

To minimize the effect of model biases on streamflow projections, we consider only the percent change in future flows relative to a historical baseline for each GCM simulation. This eliminates any absolute biases that may be present in the dynamically downscaled climate forcings. We calculate statistics for 30-year historical (1981-2010) and future (2040-2069, 2070-2099) time periods. We use 30 years because it is the convention in climate change studies – chosen as a compromise between the need to detect changes over time while minimizing sensitivity to random short-term variability.

A challenge in the current study is that 30-year periods require extrapolation to encompass the rarest events (e.g., 50-year, 100-year, 500-year). Although extrapolation leads to greater uncertainty in the flood frequency estimates, it is common practice in flood studies as we rarely have enough observed data to encompass these rare events. Nevertheless, the effects of this greater uncertainty should be considered when using the extrapolated data.

Projected changes are calculated separately for each GCM, future time period, and for each bootstrapped sub-sample. Most of our results focus on the median result from the 1,000-member bootstrap. However, we do also provide the 5$^{th}$ and 95$^{th}$ percentile values, which provide the estimated uncertainty due to sampling. The range in projections among GCMs provides an estimate of the climate model uncertainty.

## Data Access

All model results can be obtained from the project website:

https://cig.uw.edu/projects/climate-change-flooding-in-snohomish-county-new-dynamically-downscaled-hydrologic-model-projections/

Figure 13 illustrates the file structure. The DHSVM model produces an hourly streamflow time series for each streamflow site. These are included in separate files for each model: one for the WRF-OBS simulation (named "pnnl") and one for each of the WRF-GCM

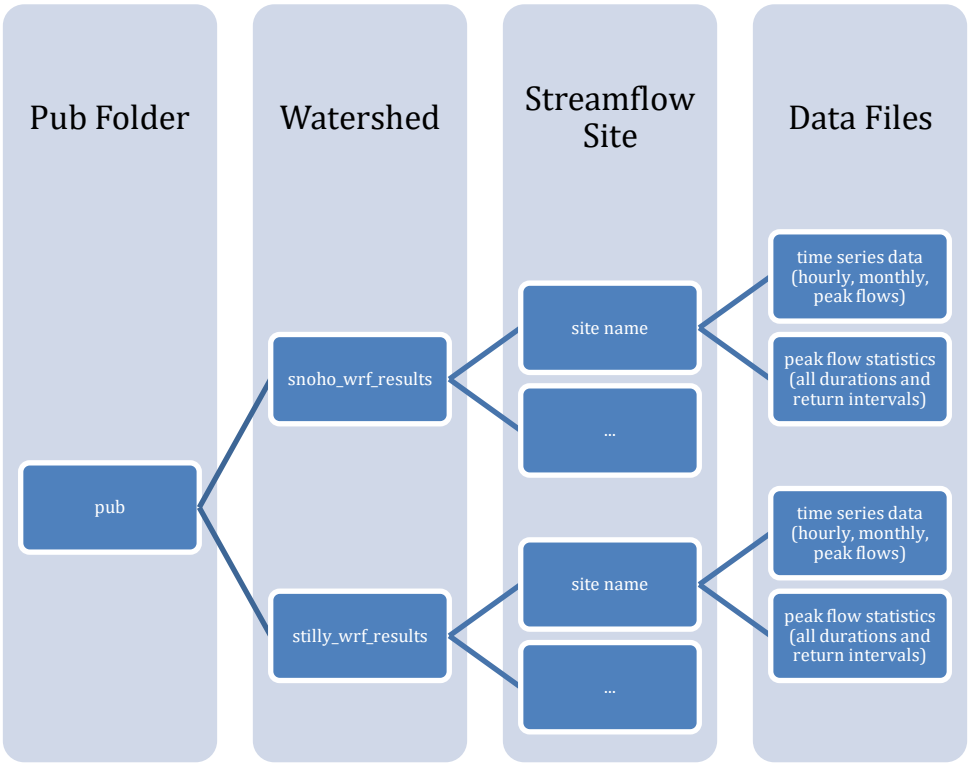


**Figure 13.** Data structure for the model results.

simulations (labeled according to the names of the GCMs listed in Table 2). A monthly time series file is similarly provided in a separate file for each model. To facilitate analyses, a number of other results are provided related to the peak flow results. These are again separated by model, duration ("1hour", "1day", "3day", "7day"), and time period ("1990s", "2050s", "2080s"). In each case two files are included: one with the peak flow time series for the duration and 30-year time period in question ("*_PeakFlows.csv"), and another with the associated peak flow statistics ("*_PeakStats.csv"). The directory for each watershed also includes a "Summary_PeakStats.csv" file that combines the percent changes in flooding for all sites, durations, and return intervals.

## Results

This section summarizes the changes in naturalized streamflow in the Snohomish and Stillaguamish River DHSVM simulations. We specify that these are naturalized flows because they do not consider the effects of water withdrawals or reservoir regulation (there are two major reservoirs in the Snohomish basin: one on the SF Tolt River, and the other on the NF Sultan River). Changes in water use, reservoir operations, or other management choices could alter flows in the future in ways that either exacerbate or mitigate the effects of climate change. Similarly, our results do not account for changes in land cover, either due to changes in management or wildfire.

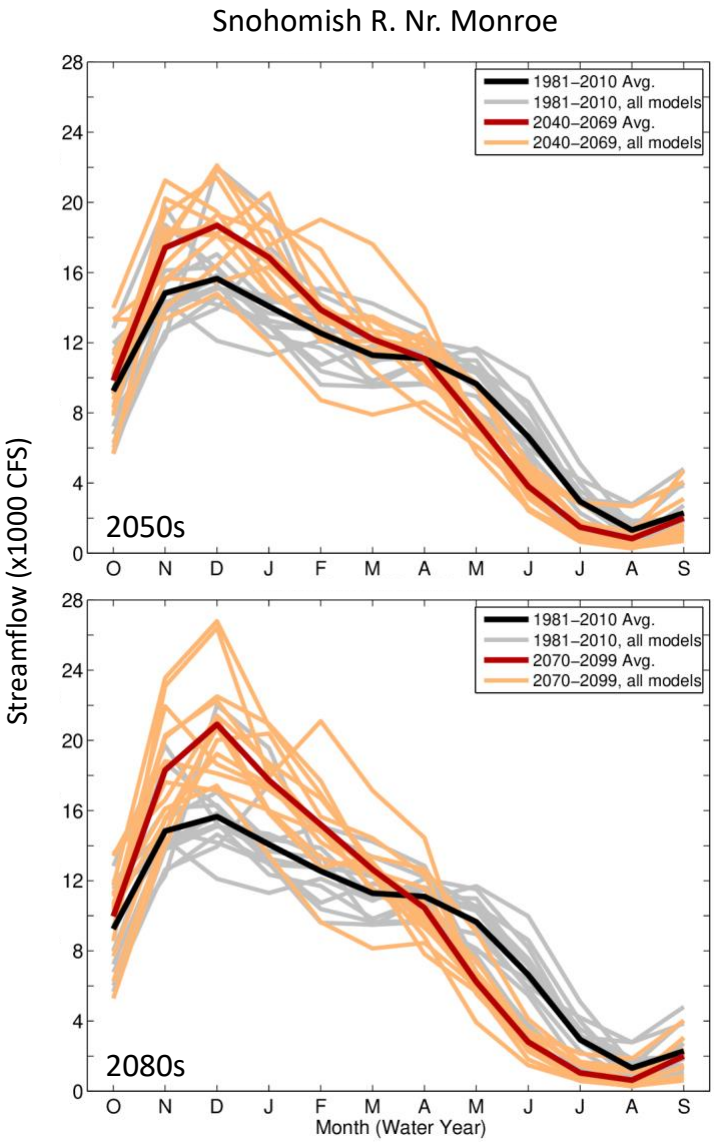


**Figure 14.** Historical and future monthly flows for the Snohomish River Near Monroe. Each line shows the results for one WRF-GCM projection. The grey lines show the historical average (1981-2010), while the yellow/red lines show the average for the 2050s (top) and the 2080s (bottom).

As discussed in previous sections, all results are based on the bias-corrected hourly WRF-GCM forcings (temperature, precipitation, humidity, wind, and shortwave radiation), and the empirical longwave estimates described above. Although the climate data are bias-corrected, no bias-correction is applied to the streamflow estimates. This is because previous studies have shown that doing so can introduce artifacts that alter

projected trends over time. To control for biases in the projections, our results focus on percent changes in streamflow (i.e., we calculate the percent change for a given GCM projection relative to the historical estimate from that same GCM). We show absolute monthly flows because these are likely to be more reliable – based on the scores shown in Tables 10 and 14 – and also because the seasonal changes in flow are easier to discern when considering absolute flows.

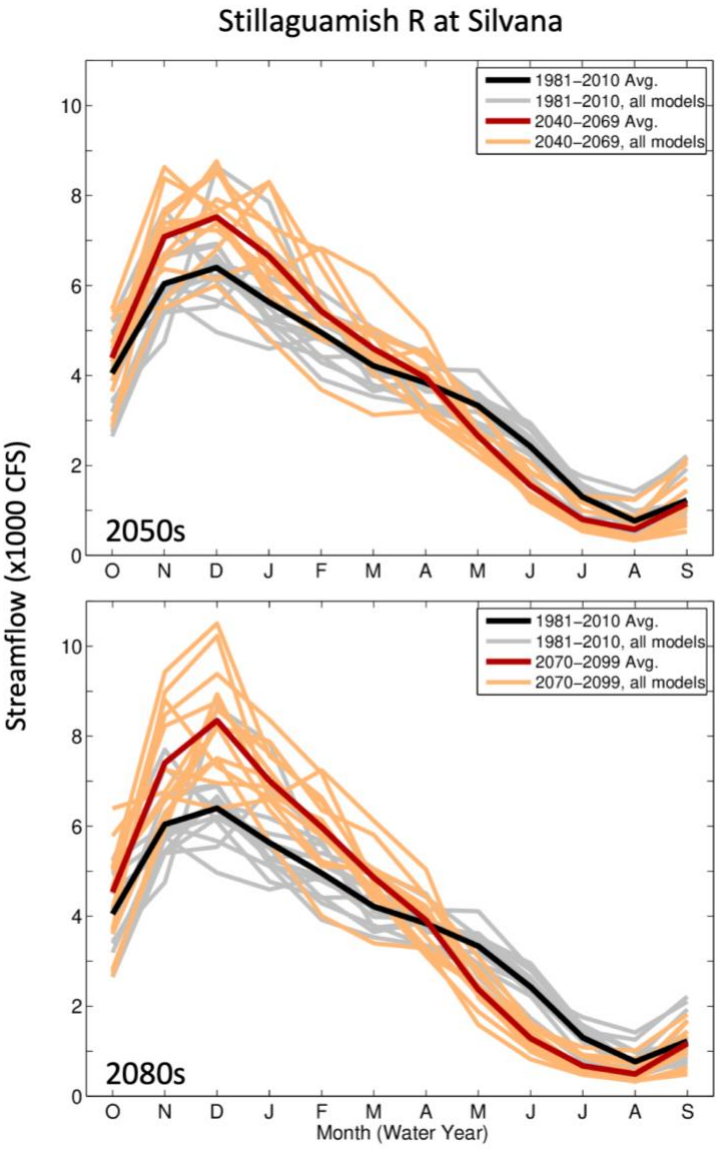


**Figure 15.** Historical and future monthly flows for the Stillaguamish River at Silvana. Each line shows the results for one WRF-GCM projection. The grey lines show the historical average (1981-2010), while the yellow/red lines show the average for the 2050s (top) and the 2080s (bottom).

## Projected Changes in Monthly Flows

Consistent with the observed and naturalized flows, historical simulations show that the Snohomish and Stillaguamish Rivers are mixed-rain-and-snow basins, where streamflow peaks in early winter due to rainfall, but also shows a secondary peak in spring due to snowmelt (Figures 14 and 15). Warming causes a greater proportion of precipitation to fall as rain, leading to increased winter flows, decreased snowpack, and decreased spring/summer flows. The result is a shift in the seasonal cycle of streamflow to a more dominant winter peak occurring in December, on average, and an earlier and significantly diminished contribution

from snowmelt occurring around April. All of the GCM scenarios considered here exhibit this change by the 2080s, and most do so by the 2050s. Although variability in seasonal and annual precipitation can cause some winters to have higher flows than others, all scenarios considered here project that the ratio of cool-season (Oct-Mar) to annual flow volume increases over time. These results are consistent with previous studies (e.g., Elsner et al. 2010, Hamlet et al. 2013), which show a clear temperature-induced trend that is modulated by precipitation variability.

## Projected Changes in Peak Flows

Peak flows in both basins are projected to increase for nearly all models, durations, return intervals, and time periods that we considered. Assessing trends in extremes is difficult, since they are by definition rare events – this undoubtedly adds some noise to the projected changes, and this noise is likely greater for the largest events (e.g., 50-year, 100-year). Our bootstrap approach to assessing extremes, described in the methods section of this report, was one attempt to minimize the effect of this sampling bias on the extreme statistics. Another approach we take is to focus on the smaller, more frequent, extreme events, since these are likely well-captured by our 30-year sampling periods and therefore less influenced by natural variability.

Results for the Snohomish and Stillaguamish Rivers are discussed separately below. The findings for both watersheds are similar.

### *Snohomish River*

Figure 16 shows the projected changes in peak streamflow magnitude for the 2-year event at nine different gauging stations throughout the Snohomish watershed. These results show general consistency in the average projections, but large uncertainty around those averages. There also appears to be some tendency for the projected increases to be larger for longer durations, though this is not universal across all sites. Although there are differences in the average projections for each site, they are small compared to the range among model projections and do not exhibit a clear geographic pattern. The range among models, however, tends to be greater for smaller, higher-elevation tributaries. Based on our analysis (not shown), we do not recommend using the projected changes in the 1.01-

and 500-year event frequencies. Instead, we recommend using the projected change for the more frequent events (e.g., 2-, 5-, 10-year events), or the average projected change across several return frequencies. For example, Table 15 shows the projected changes obtained by averaging among the projections for the 2-, 5-, 10-, 25-, 50-, and 100-year events. These echo the results shown in Figure 16, showing relatively similar average projections across all sites, with greater ranges at the high elevation sites and generally higher projections for the 1-hour duration, when compared to the 1-day duration.

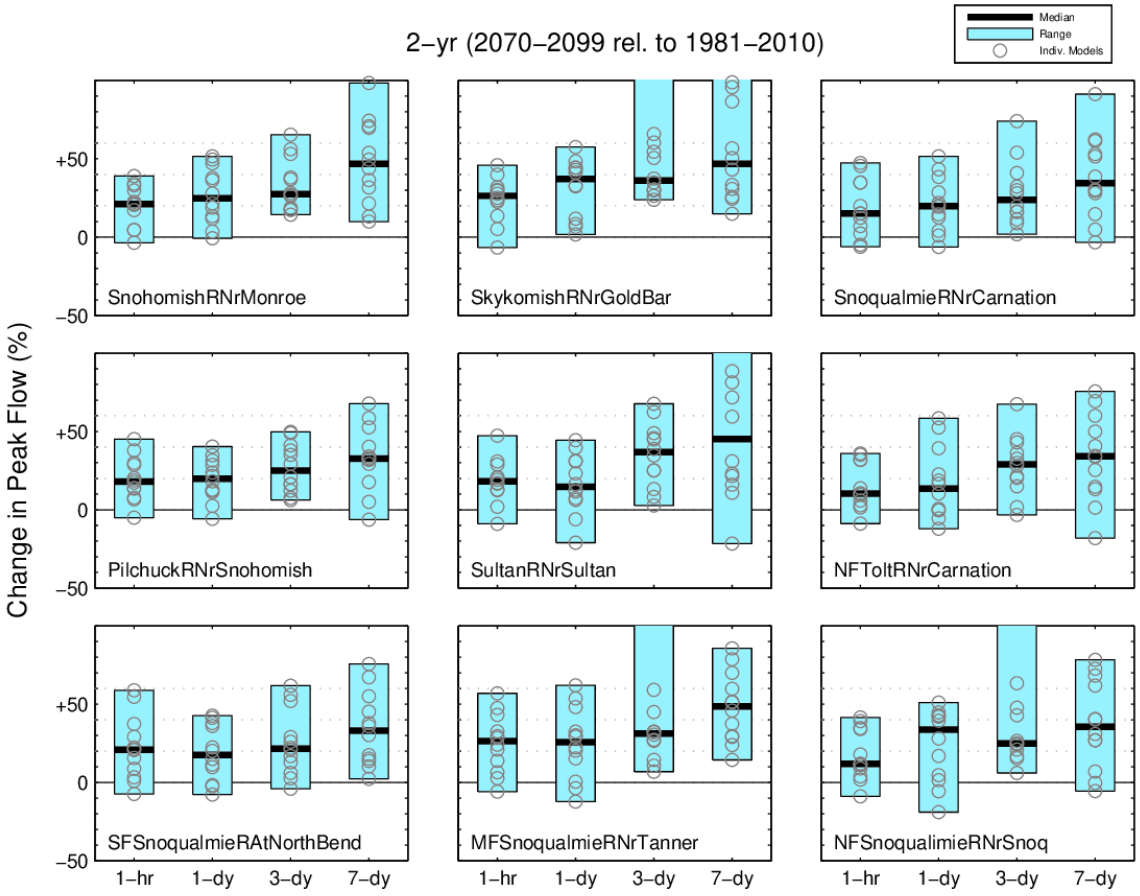


**Figure 16.** Projected change in the 2-year event, for four durations and nine gauge locations in the Snohomish River basin. Projected changes are shown for the 2080s (2070-2099) relative to 1981-2010. The black lines show the median, bars show the range, and circles the individual model results.

**Table 15.** Average projected change in peak flows, obtained by averaging the model results for the 2-, 5-, 10-, 25-, 50-, and 100-year events. Results are included for 11 gauge sites in the Snohomish basin, for the 2080s (2070-2099) relative to 1981-2010.

| Station | Durn. | Avg. | 25th / 75th | min / max |
|---|---|---|---|---|
| SF Snoq. R. at North Bend | 1 hr | +28% | +11% / +48% | -1% / +58% |
| | 1 day | +27% | +11% / +41% | -4% / +52% |
| MF Snoq. R. nr. Tanner | 1 hr | +29% | +14% / +44% | +4% / +55% |
| | 1 day | +28% | +13% / +41% | +5% / +53% |
| NF Snoq. R. nr. Snoq. Falls | 1 hr | +25% | +12% / +38% | -7% / +60% |
| | 1 day | +21% | +6% / +36% | -4% / +45% |
| Snoq. R. nr. Snoqualmie | 1 hr | +27% | +11% / +42% | -1% / +54% |
| | 1 day | +25% | +10% / +41% | -0% / +46% |
| Raging R. nr. Fall City | 1 hr | +25% | +4% / +53% | -1% / +58% |
| | 1 day | +15% | +5% / +30% | -11% / +41% |
| NF Tolt R. nr. Carnation | 1 hr | +21% | +10% / +34% | -15% / +58% |
| | 1 day | +19% | -3% / +42% | -14% / +57% |
| Snoq. R. nr. Carnation | 1 hr | +26% | +8% / +44% | -6% / +50% |
| | 1 day | +24% | +10% / +40% | -2% / +41% |
| Sultan R. nr. Sultan | 1 hr | +21% | +14% / +29% | -4% / +37% |
| | 1 day | +25% | +12% / +36% | -14% / +57% |
| Skykomish R. nr. Gold Bar | 1 hr | +22% | +17% / +30% | -8% / +49% |
| | 1 day | +27% | +14% / +40% | -1% / +53% |
| Snohomish R. nr. Monroe | 1 hr | +24% | +17% / +36% | -8% / +45% |
| | 1 day | +24% | +16% / +36% | -3% / +45% |
| Pilchuck R. nr. Snohomish | 1 hr | +23% | +14% / +35% | -5% / +48% |
| | 1 day | +23% | +12% / +41% | -13% / +52% |

*Stillaguamish River*

Figure 17 shows the projected changes in peak streamflow magnitude for the 2-year event at nine different gauging stations throughout the Stillaguamish watershed. These results show significant variability; however, there appears to be some tendency for the projected increases to be larger for longer durations, though this is not universal across all sites or event sizes. For very rare events (e.g., 50 or 100-yr peak flows), this trend seems to reverse

with longer durations, showing nominal increases for longer durations but significant increases for shorter durations (not shown). This may be indicative of a change in streamflow mechanisms due to warming (i.e., smaller rain on snow impulses from a reduced snowpack) or it may be noise: an artifact of extrapolation from our 30-year period of comparison. As in the Snohomish basin, there are only very slight spatial variations in the average projections. The range among models, however, tends to be greater for smaller, higher-elevation tributaries.

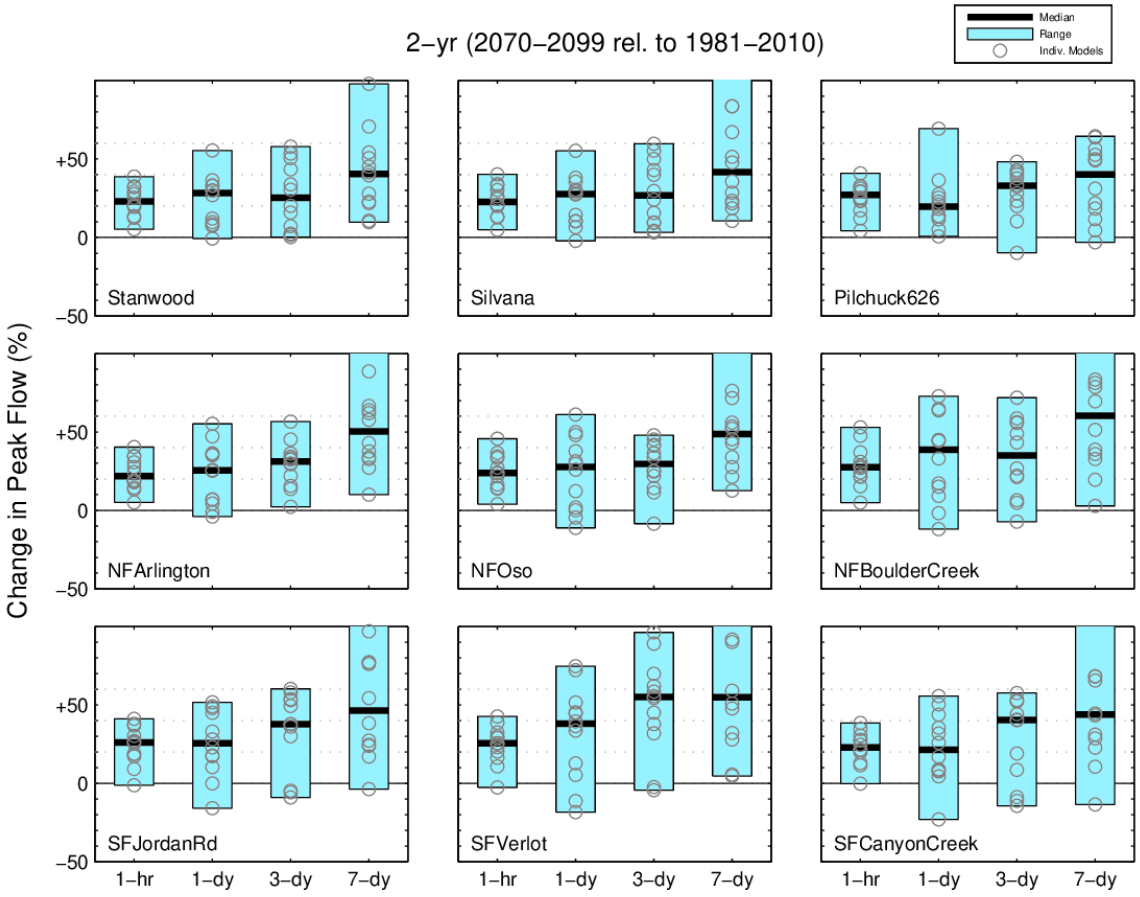


**Figure 17.** Projected change in the 2-year event, for four durations and nine gauge locations in the Stillaguamish River basin. Projected changes are shown for the 2080s (2070-2099) relative to 1981-2010. The black lines show the median, bars show the range, and circles the individual model results.

Table 16 shows the projected changes obtained by averaging among the projections for the 2-, 5-, 10-, 25-, 50-, and 100-year events. These mirror the results shown in Figure 17, showing relatively similar average projections across all sites, with greater ranges at the high elevation sites and generally higher projections for the 1-day duration, when compared to the 1-hour duration.

**Table 16.** Average projected change in peak flows, obtained by averaging the model results for the 2-, 5-, 10-, 25-, 50-, and 100-year events. Results are included for 12 sites in the Stillaguamish basin, for the 2080s (2070-2099) relative to 1981-2010.

| Station | Durn. | Avg. | 25th / 75th | min / max |
|---|---|---|---|---|
| Stillaguamish R at Stanwood | 1 hr | +29% | +19% / +41% | +6% / +45% |
| | 1 day | +24% | +19% / +32% | -5% / +41% |
| Stillaguamish R at Silvana | 1 hr | +27% | +18% / +40% | +5% / +43% |
| | 1 day | +25% | +17% / +34% | -6% / +48% |
| Pilchuck Creek at Br 626 | 1 hr | +33% | +23% / +44% | +4% / +66% |
| | 1 day | +29% | +15% / +42% | -2% / +53% |
| NF Stillaguamish R nr Arlington | 1 hr | +25% | +14% / +36% | +2% / +40% |
| | 1 day | +28% | +22% / +31% | -6% / +60% |
| NF Stillaguamish R nr Oso | 1 hr | +21% | +12% / +32% | -0% / +37% |
| | 1 day | +28% | +18% / +36% | -6% / +64% |
| NF Stillaguamish R nr Darrington | 1 hr | +17% | +10% / +28% | -11% / +34% |
| | 1 day | +29% | +22% / +39% | -6% / +71% |
| Deer Creek at mouth to NF | 1 hr | +24% | +17% / +33% | -3% / +37% |
| | 1 day | +28% | +17% / +38% | +3% / +43% |
| Boulder Creek at mouth to NF | 1 hr | +26% | +17% / +36% | +8% / +38% |
| | 1 day | +40% | +29% / +55% | -4% / +82% |
| SF Stillaguamish R nr Jordan Rd | 1 hr | +26% | +20% / +36% | +6% / +41% |
| | 1 day | +32% | +20% / +47% | -11% / +61% |
| SF Stillaguamish R nr Verlot | 1 hr | +22% | +15% / +29% | +5% / +36% |
| | 1 day | +37% | +24% / +50% | -6% / +73% |
| Jim Creek at mouth to SF | 1 hr | +30% | +20% / +36% | +9% / +61% |
| | 1 day | +26% | +11% / +47% | -10% / +66% |
| Canyon Creek at mouth to SF | 1 hr | +24% | +15% / +32% | +7% / +38% |
| | 1 day | +32% | +20% / +38% | -7% / +78% |

## Conclusions

There are two primary pathways for climate change to influence river flooding in the Snohomish and Stillaguamish watersheds: (1) decreasing snowpack and (2) higher intensity precipitation events. Snowpack declines lead to increased flooding by increasing the portion of the watershed that receives rain during winter storm events. This increase in the proportion of rainfall relative to snowfall relates directly to the volume of water supplied to streams and rivers during a flood event. Snowpack has already declined significantly over recent decades and is projected to continue declining throughout this century (Mote et al. 2018). This is a consequence of climate change that will be important over the near-term as the two basins transition from mixed-rain-and-snow to rain-dominant – Figures 14 and 15 show that the rain dominance is evident by the 2050s. Heavy rain events are projected to become more intense particularly in the second half of this century (Warner et al. 2015). As with the declines in winter snowpack, this translates directly into more water in streams during flood events. Changes in rainfall intensity will be more important later in the century; near-term changes are likely to be primarily a consequence of declining snowpack.

Overall, our results indicate that peak flows will increase substantially – ranging from about +10 to +40%, on average, depending on the specific tributary or river location in question. Our results also show a tendency for larger changes, and a wider range among projections, for longer duration flood events. The results do not show a clear relationship with return interval (e.g., 2-year vs 100-year events).

### Interpreting the results

Interpretation of these results, particularly given the focus on rare extreme events, can be challenging. Following are a few considerations to keep in mind when reviewing the results:

- Projected changes will always be governed by a combination of random variability and long-term trends due to climate change. We based our projections on 30-year time periods, since averaging over 30 years is likely to significantly reduce the effect of natural variability. Nonetheless, it is possible that multi-decadal variations in climate can obscure trends in some instances. We recommend considering multiple lines of evidence (e.g., multiple return intervals and durations) before concluding that a particular trend is to be expected.

- By definition, extreme events are rare. This makes it difficult to assess how rapidly they change. In particular, our use of 30-year periods limits the return intervals that can be reliably quantified. The 50-, 100-, and 500-year events can only be estimated by extrapolating from the GEV distribution. Even the 15-year event could be under-sampled, given that it would only occur twice, on average, in each 30-year time period. Our bootstrap approach should help reduce the effects of outliers. Nonetheless, we recommend focusing on the results for the 2-, 5-, and 10-year events, or averaging results across multiple return frequencies (e.g., 2-year through 100-year event projections) until a more robust approach can be developed for estimating trends in the rarest events.
- The WRF model used in this study has a spatial resolution of 12 km. While much better than the resolution afforded by GCMs, this is still coarse relative to some weather and topographic features. For example, thunderstorms are not resolved at a resolution of 12 km. Although we do not think thunderstorms are an important driver of flood risk in the basin, it is possible that other variations in weather conditions could have an important influence on flows.
- A limitation of complex hydrologic models such as DHSVM is that there are more parameters to tune than there are observations with which to constrain them. This means that it is possible for calibration to lead to "the right answer for the wrong reason". This is an especially challenging issue with climate change, since a model that performs well under current conditions may not be able to accurately capture changes in flow under future climate conditions. We have tested the model calibration in multiple ways in order to avoid this pitfall, but cannot be sure that the issue does not remain.
- The DHSVM model is not able to capture deep or confined groundwater. Recent research suggests that deep groundwater could be an important contributor to summer low flows on the Snoqualmie River (McGill et al. 2021). While important to low flows, groundwater is unlikely to be important for peak flows.
- In a recent study comparing evapotranspiration estimates, Milly and Dunne (2017) found that most hydrologic models dramatically overestimate future changes in evapotranspiration. This includes the Penman-Monteith method used in DHSVM. This is not likely to be an issue for peak flow simulations. However, this could have

important implications for summer flows, and would be important to estimate correctly in any future study evaluating the implications of possible changes in land cover.

- The streamflow projections are based on current landcover conditions. Forestry practices and further urbanization could also significantly affect future flows, as could increases in the frequency and extent of wildfire due to climate change. Modifications to the land cover in DHSVM, or the new canopy gap option in DHSVM version 3.2, could both be used to assess forest harvest impacts in future modeling assessments. Current work by the Tulalip Tribe is investigating some of these potential impacts.
- Our results concern changes in naturalized flows (i.e.: no reservoirs or water withdrawals). Reservoir management practices in the Snohomish watershed could have significant effects on peak flows on the tributaries with dams (NF Sultan River, SF Tolt River), but that influence becomes progressively less important moving downstream from the confluence with the mainstem Skykomish and Snoqualmie Rivers. There are presently no dams or reservoirs within the Stillaguamish watershed.
- This project has focused on quantifying the changes in streamflow and water temperature due to climate change. To assess climate vulnerability, two other pieces of information are needed: (1) the "sensitivity" to these changes – how impacts scale with future changes, and (2) the "adaptive capacity" – how much these changes can be mitigated by changes in land use and water management or salmonid life history characteristics. Work to better understand these complementary aspects of vulnerability would help clarify if, when, and where to focus efforts at managing climate change risks.

## Future Work

The science of climate change will continue to evolve over time due to changes in greenhouse gas scenarios, global climate models, downscaling approaches, and the hydrologic modeling used to make localized streamflow projections. In addition, further refinements to the existing approach could result in improved model estimates of current and future conditions. Future work could also further refine the approaches used to develop meteorological forcings and tune the DHSVM model.

Planning requires more than just understanding the implications of climate change. Managers need to know which interventions are likely to be needed, which are most effective, and how the answers to these questions vary across the watershed. Now that these models have been developed and calibrated, some questions can be answered more easily. For example, the existing models presented in this study can be used to look at the implications of land cover change on streamflow. Similarly, additional work could build on the DHSVM modeling to model the implications for future water temperatures, or regulated peak flows downstream of reservoirs.

The domain of the regional climate model used to develop these projections covers the entire Pacific Northwest, stretching from northern California to British Columbia and from the west coast through the Rocky Mountains of Montana and Wyoming. This means that the approach we used here could be evaluated for other communities around the region. For example, efforts are ongoing to develop similar projections for the about a dozen Puget Sound watersheds, including the Nooksack, Green, Puyallup, and Dungeness rivers. As interest in this work grows, additional coordination may be warranted to capitalize on economies of scale.

## References

Andreadis, K. M., Storck, P., & Lettenmaier, D. P. (2009). Modeling snow accumulation and ablation processes in forested environments. Water resources research, 45(5).

Bowling, L. C., & Lettenmaier, D. P. (2001). The effects of forest roads and harvest on catchment hydrology in a mountainous maritime environment. Water Science and Application, 2, 145-164.

Beckers, J., & Alila, Y. (2004). A model of rapid preferential hillslope runoff contributions to peak flow generation in a temperate rain forest watershed. Water Resources Research, 40(3). https://doi.org/10.1029/2003WR002582

Cardno. (2021). Lower Skykomish River Geomorphic Assessment. Prepared for Snohomish County Public Works, Everett, WA, January 29, 2021. Available from: https://www.snohomishcountywa.gov/5763/Flood-Hazard-Mapping

Clarke, K. (2020). Modeling the effects of climate change on streamflow and stream temperature in the South Fork of the Stillaguamish River. WWU Graduate School Collection. 983. http://cedar.wwu.edu/wwuet/983

Cristea, N. C., Lundquist, J. D., Loheide, S. P., Lowry, C. S., & Moore, C. E. (2014). Modelling how vegetation cover affects climate change impacts on streamflow timing and magnitude in the snowmelt-dominated upper Tuolumne Basin, Sierra Nevada. Hydrological processes, 28(12), 3896-3918.

Cuo, L., Lettenmaier, D. P., Alberti, M., & Richey, J. E. (2009). Effects of a century of land cover and climate change on the hydrology of the Puget Sound basin. Hydrological Processes: An International Journal, 23(6), 907-933.

Cuo, L., Beyene, T. K., Voisin, N., Su, F., Lettenmaier, D. P., Alberti, M., & Richey, J. E. (2011). Effects of mid-twenty-first century climate and land cover change on the hydrology of the Puget Sound basin, Washington. Hydrological Processes, 25(11), 1729-1753.

Currier, W. R., Thorson, T., & Lundquist, J. D. (2017). Independent evaluation of frozen precipitation from WRF and PRISM in the Olympic Mountains. Journal of Hydrometeorology, 18(10), 2681-2703. https://doi.org/10.1175/JHM-D-17-0026.1

Dickerson-Lange, S.E., and Mitchell, R. (2013). Modeling the effects of climate change projections on streamflow in the Nooksack River basin, Northwest Washington: Hydrological Processes, v. 28, p. 5236–5250, doi:10.1002/hyp.10012.

Dilley, A. C., & O'brien, D. M. (1998). Estimating downward clear sky long-wave irradiance at the surface from screen temperature and precipitable water. Quarterly Journal of the Royal Meteorological Society, 124(549), 1391-1401.

Du, E., Link, T. E., Gravelle, J. A., & Hubbart, J. A. (2014). Validation and sensitivity test of the distributed hydrology soil-vegetation model (DHSVM) in a forested mountain watershed. Hydrological Processes, 28(26), 6196–6210. https://doi.org/10.1002/hyp.10110

Dubin, A. M., and D.P. Lettenmaier (1999). Assessing the influence of digital elevation model resolution on hydrologic modeling, Water Resources Series, Technical Report 159, University of Washington, Seattle.

Elsner, M. M., Cuo, L., Voisin, N., Deems, J. S., Hamlet, A. F., Vano, J. A., & Lettenmaier, D. P. (2010). Implications of 21st century climate change for the hydrology of Washington State. Climatic Change, 102(1), 225-260.

Freeman, K. (2019). Modeling the effects of climate variability on hydrology and stream temperatures in the North Fork of the Stillaguamish River. WWU Graduate School Collection. 855. http://cedar.wwu.edu/wwuet/855

Gupta, H. V., Kling, H., Yilmaz, K. K., & Martinez, G. F. (2009). Decomposition of the mean squared error and NSE performance criteria: Implications for improving hydrological modelling. Journal of hydrology, 377(1-2), 80-91.

Hinkelman, L. M., Lapo, K. E., Cristea, N. C., & Lundquist, J. D. (2015). Using CERES SYN surface irradiance data as forcing for snowmelt simulation in complex terrain. Journal of Hydrometeorology, 16(5), 2133-2152.

Homer, Collin G., Dewitz, Jon A., Jin, Suming, Xian, George, Costello, C., Danielson, Patrick, Gass, L., Funk, M., Wickham, J., Stehman, S., Auch, Roger F., Riitters, K. H., Conterminous United States land cover change patterns 2001–2016 from the 2016 National Land Cover Database: ISPRS Journal of Photogrammetry and Remote Sensing, v. 162, p. 184–199, at https://doi.org/10.1016/j.isprsjprs.2020.02.019

Jin, S., Homer, C.G., Yang, L., Danielson, P., Dewitz, J., Li, C., Zhu, Z., Xian, G., and Howard, D. (2019). Overall methodology design for the United States National Land Cover Database 2016 products. Remote Sensing, 11(24); https://doi.org/10.3390/rs11242971

Mauger, G.S., S.-Y. Lee, C. Bandaragoda, Y. Serra, J.S. Won, (2016). Refined Estimates of Climate Change Affected Hydrology in the Chehalis basin. Report prepared for Anchor QEA, LLC. Climate Impacts Group, University of Washington, Seattle. https://doi.org/10.7915/CIG53F4MH

McGill, L. M., Brooks, J. R., & Steel, E. A. (2021). Spatiotemporal dynamics of water sources in a mountain river basin inferred through δ2H and δ18O of water. Hydrological Processes, 35(3), e14063.

Minder, J. R., Mote, P. W., & Lundquist, J. D. (2010). Surface temperature lapse rates over complex terrain: Lessons from the Cascade Mountains. Journal of Geophysical Research: Atmospheres, 115(D14). https://doi.org/10.1029/2009JD013493

Mote, P. W., Li, S., Lettenmaier, D. P., Xiao, M., & Engel, R. (2018). Dramatic declines in snowpack in the western US. Npj Climate and Atmospheric Science, 1(1), 1-6.

Nash, J.E., and Sutcliffe, J.V. (1970). River flow forecasting through conceptual models part I — A discussion of principles: Journal of Hydrology, v. 10, p. 282–290, doi:10.1016/0022-1694(70)90255-6.

Naz, B. S., Frans, C. D., Clarke, G. K. C., Burns, P., & Lettenmaier, D. P. (2014). Modeling the effect of glacier recession on streamflow response using a coupled glacio-hydrological model. Hydrology and Earth System Sciences, 18(2), 787-802.

Nick, M., Das, S. and Simonovic, S.P. (2011). The Comparison of GEV, Log-Pearson Type 3 and Gumbel Distributions in the Upper Thames River Watershed under Global Climate Models, the University of Western Ontario Department of Civil and Environmental Engineering, Report No:077.

NOAA. (2019). Washington State Landcover Data Set, 2016. Coastal Change Analysis Program (C-CAP). Charleston, SC: NOAA Office for Coastal Management. Accessed November 2019 via: https://coast.noaa.gov/ccapftp/#/

NRCS, (2017). Soil Survey Staff, Natural Resources Conservation Service, United States Department of Agriculture. Web Soil Survey. Available online at http://websoilsurvey.nrcs.usda.gov/. Accessed in 2017.

Prata, A. J. (1996). A new long-wave formula for estimating downward clear-sky radiation at the surface. Quarterly Journal of the Royal Meteorological Society, 122(533), 1127–1151. https://doi.org/10.1002/qj.49712253306

Rahman, A., Weinmann, P.E. and Mein, R.G. (1999). At-site flood frequency analysis: LP3-product moment, GEV-L moment and GEV-LH moment procedures compared. In: Proceeding Hydrology and Water Resource Symposium, Brisbane, 6–8 July, 2, 715–720.

Rahman, A., Karin, F, and Rahman, A. (2015). Sampling Variability in Flood Frequency Analysis: How Important is it? 21st International Congress on Modelling and Simulation, Gold Coast, Australia, Nov 29-Dec 4, 2015, 2200-2206.

Salathé Jr, E. P., Hamlet, A. F., Mass, C. F., Lee, S. Y., Stumbaugh, M., & Steed, R. (2014). Estimates of 21st century flood risk in the Pacific Northwest based on regional climate model simulations. Journal of Hydrometeorology, (2014).

Storck, P., Bowling, L., Wetherbee, P., & Lettenmaier, D. (1998). Application of a GIS-based distributed hydrology model for prediction of forest harvest effects on peak stream flow in the Pacific Northwest. Hydrological Processes, 12(6), 889-904.

Storck, P. (2000). Trees, snow and flooding: An investigation of forest canopy effects on snow accumulation and melt at the plot and watershed scales in the Pacific Northwest.

Storck, P., Lettenmaier, D. P., & Bolton, S. M. (2002). Measurement of snow interception and canopy effects on snow accumulation and melt in a mountainous maritime climate, Oregon, United States. Water Resources Research, 38(11), 5-1.

Sun, N., Yearsley, J. R., & Lettenmaier, D. P. (2013). Predicting the Effect of Changing Precipitation Extremes and Land Cover Change on Urban Water Quality. In AGU Fall Meeting Abstracts (Vol. 2013, pp. H31H-1312).

Sun, N., Wigmosta, M., Zhou, T., Lundquist, J., Dickerson-Lange, S., and Cristea, N. (2018). Evaluating the functionality and streamflow impacts of explicitly modelling forest–

snow interactions and canopy gaps in a distributed hydrologic model: Hydrological Processes, v. 32, p. 2128–2140, doi:10.1002/hyp.13150.

Sun, N., Yan, H., Wigmosta, M.S., Leung, L.R., Skaggs, R., and Hou, Z. (2019). Regional Snow Parameters Estimation for Large-Domain Hydrological Applications in the Western United States: Journal of Geophysical Research: Atmospheres, v. 124, p. 5296–5313, doi:10.1029/2018JD030140.

Taylor, K. E., Stouffer, R. J., & Meehl, G. A. (2012). An overview of CMIP5 and the experiment design. Bulletin of the American meteorological Society, 93(4), 485-498. https://doi.org/10.1175/BAMS-D-11-00094.1

Tohver, I. M., Hamlet, A. F., & Lee, S. Y. (2014). Impacts of 21st-Century Climate Change on Hydrologic Extremes in the Pacific Northwest Region of North America. JAWRA Journal of the American Water Resources Association, 50(6), 1461-1476.

Unsworth, M. H., & Monteith, J. L. (1975). Long-wave radiation at the ground I. Angular distribution of incoming radiation. Quarterly Journal of the Royal Meteorological Society, 101(427), 13-24. https://doi.org/10.1002/qj.49710142703

Van Vuuren, D. P., Edmonds, J., Kainuma, M., Riahi, K., Thomson, A., Hibbard, K., ... & Rose, S. K. (2011). The representative concentration pathways: an overview. Climatic change, 109(1), 5-31. https://doi.org/10.1007/s10584-011-0148-z

Vogel, R.M., McMahon, T.A. and Chiew, F.H.S. (1993). Flood flow frequency model selection in Australia, Journal Hydrology, 146, 421-449.

Warner, M. D., Mass, C. F., & Salathe Jr, E. P. (2015). Changes in winter atmospheric rivers along the North American west coast in CMIP5 climate models. Journal of Hydrometeorology, 16(1), 118-128.

Whitaker, A., Alila, Y., Beckers, J., & Toews, D. (2003). Application of the distributed hydrology soil vegetation model to Redfish Creek, British Columbia: model evaluation using internal catchment data. Hydrological processes, 17(2), 199-224.

Wigmosta, M. S., & Lettenmaier, D. P. (1999). A comparison of simplified methods for routing topographically driven subsurface flow. Water Resources Research, 35(1), 255-264.

Wigmosta, M. S., Nijssen, B., Storck, P., & Lettenmaier, D. P. (2002). The distributed hydrology soil vegetation model. Mathematical models of small watershed hydrology and applications, 7-42.

WSE (Watershed Science and Engineering). (2021). Hydraulic and Hydrologic Modeling in the Snohomish Watershed, prepared for Snohomish County Public Works, Everett, WA, April 2021. Available from: https://www.snohomishcountywa.gov/5763/Flood-Hazard-Mapping

Yang, Limin, Jin, Suming, Danielson, Patrick, Homer, Collin G., Gass, L., Bender, S.M., Case, Adam, Costello, C., Dewitz, Jon A., Fry, Joyce A., Funk, M., Granneman, Brian J., Liknes, G.C., Rigge, Matthew B., Xian, George (2018). A new generation of the United States National Land Cover Database—Requirements, research priorities, design, and implementation strategies: ISPRS Journal of Photogrammetry and Remote Sensing, v. 146, p. 108–123, at https://doi.org/10.1016/j.isprsjprs.2018.09.006

Yapo, P. O., H. V. Gupta, S. Sorooshian, (1998). Multi-objective global optimization for hydrologic models, J. Hydrol., 204, 83–97.